Revising the formation of β-hematin crystals from hemin in aqueous-acetate medium containing chloroquine: modeling the kinetics of crystallization and characterizing their physico-chemical properties

Leidy J. Herrera [1], Cristián A. Parra[2], Daniel Coronado[3], Valentina Pérez [1], Julián A. Zapata[3], Adriana L. Pabón[4], Olga Lopez-Acevedo [2], Karen E. García[1], César A. Barrero[1,]*

[1]Solid State Research Group, Faculty of Exact and Natural Sciences, University of Antioquia-UdeA, Calle 70 No. 52-21, Medellín, Colombia.

[2]Max Planck Tandem Group Biophysics of Tropical Diseases, Faculty of Exact and Natural Sciences, University of Antioquia-UdeA, Calle 70 No. 52-21, Medellín, Colombia.

[3]Residue Analysis Research Group, Faculty of Exact and Natural Sciences, University of Antioquia-UdeA, Calle 70 No. 52-21, Medellín, Colombia.

[4]Malaria Group, Faculty of Medicine, University of Antioquia-UdeA, Medellín, Colombia.

**Author of correspondence: cesar.barrero@udea.edu.co*

ABSTRACT

We investigated the kinetics of conversion of hemin to β-hematin in aqueous-acetate medium in absence and in presence of two concentrations of chloroquine by using eleven reported kinetic equations. The two best kinetic equations are the combination of order 1 and Avrami and the combination of second order and logistic equations, based on the statistical parameters variance and overall errors. The best fitted equations are composed of two terms from which we model the formation of β-hematin as the result of two processes: the availability of reactive precursors and the formation of nucleation and growth sites. The crystals exhibit needle-like morphologies of about 760 nm long and 140 nm wide. However, the increment of chloroquine favors the formation of crystal twinning with non-homogenous distribution, crystals with lower sizes of similar heights and widths, and crystals symmetrically tapered at the ends of the needles. The lattice volumes, obtained from Rietveld analysis of powder X-ray diffraction patterns, were not regularly affected by chloroquine. The main IR absorption bands did not appreciably change in positions nor in intensities with varying chloroquine concentration. However, important changes were observed in the 2000-4000 cm^{-1} region. We used Density Functional Theory calculations to understand these changes.

KEYWORDS:

Kinetics of formation, β-hematin crystals, hemin, chloroquine, morphology, powder X-ray diffraction (PXRD).

INTRODUCTION

Plasmodium is a parasite that is transmitted to man by the bite of a mosquito of the genus Anopheles and causes malaria. This remains a significant public health problem. The World Malaria Report 2021 estimated that the global malaria burden was around 241 million reported cases and 496 000 deaths worldwide. To date there are six species of Plasmodium that affect humans, however, *P. vivax* and *P. falciparum* are the most important. *P. vivax* is widely distributed and occurs mainly in the Americas and *P. falciparum* is the species that causes the highest number of complications and deaths.[1]

During the life cycle of Plasmodium in the human host, it has an intraerythrocytic phase, which is related to the symptoms of the disease. In this cycle, Plasmodium degrades hemoglobin and after several processes forms the hemozoin crystal, or malaria pigment. It is widely accepted that the formation of the hemozoin in the digestive vacuole of the Plasmodium parasite is the primary mechanism of heme detoxification in the malaria parasites and the target of quinoline type of antimalarials.[2–4] Therefore, it is very important to have a deep understanding of the formation mechanisms and kinetics of nucleation and growth of the hemozoin crystals and their inhibition by the antimalarial medicines. These types of studies have been performed on both natural and synthetic samples, the methods being valuable and complementary.

The synthetic version of the hemozoin crystal is called β-hematin, and it can be synthesized under widely different conditions. One of the earliest reactive mediums used to synthesize β-hematin was acidic acetate solutions.[5–8] Egan and co-workers[5,6] reported short reaction

times for the formation of about 30 min under the reaction conditions of 4,5 M acetate buffer, pH 4,5 and 60°C. The reaction was also complete within 2 hours at 37°C, and 8 days at 6°C. In 1993, Bohle and Helms[9] reported that β-hematin can also be obtained by abstraction of HCl from hemin with non-coordinated base in strictly anhydrous conditions. Fitch et al.[10] investigated the involvement of lipids and detergents in the formation of β-hematin, finding that some of these promote crystal formation. In a complementary work, Hoang et al.[11] employed a model system consisting of an emulsion of neutral lipid particles to study the crystallization process at conditions that mimic the chemical environment of the parasite's digestive vacuole.[12] In another related work, Hoang and co-workers[13] concluded that the lipid blend strongly promotes β-hematin formation by drastically lowering the activation energy of the process. Other several works have been reported using detergents,[14–17] alcohols,[18,19] mixtures of organic solvents like methanol/CCl_4,[19] and different buffer systems, for example, the citric buffer-saturated n-octanol (CBSO) reported by Vekilov and co-workers.[20] In general, from the studies mentioned above, there are two main factors in the medium composition that affect the kinetics of β-hematin crystallization: the presence of a buffer system with a pH in the range between 4 and 5, and the presence of aqueous/organic regions with a low surface tension.

In addition to the selection of a proper reaction medium, a minimal chemical mechanism for the kinetics of β-hematin formation and inhibition is highly desirable. This equation, that describes the chemical mechanism, should allow a prediction of the rate of formation of the crystals, which is a crucial factor for understanding the mechanisms of crystallization

and inhibition. Several kinetic equations have been reported in the literature. Adams et al.[21] reported that spontaneous formation of β-hematin from hematin in acetate solution follows pseudo-zero-order and not autocatalytic kinetics. The pseudo-zero-order model implies that the β-hematin formation does not depend on the concentration of Hemin. Late, Egan et al.[22] analyzed the kinetic curves using the first order kinetic, the results obtained by them suggest that β-hematin formation depends on the concentration of hematin. In a previous work, Egan et al.[8] also reported the formation of β-hematin from hematin in acidic acetate solution and fit the kinetic curves with the Avrami model.[23] In this model, crystallization is the result of nucleation and growth processes. According to Egan et al.[8] the acetate medium may act as a phase transfer catalyst, solubilizing hematin and facilitating its redeposition as β-hematin. The formation proceeds by rapid precipitation of amorphous hematin, followed by slow conversion to crystalline β-hematin. In an attempt to explicitly include the effects of the quinoline antimalarials in the kinetics of formation, Egan and Ncokazi[24] incorporated the concentration of the antimalarial as a variable in one term of the Avrami equation.

On the other hand, Gildenhuys et al.[25] proposed a kinetic model that combines the crystallization characteristics of Avrami equation, and the interaction between the surface of the crystal and the antimalarial medicine in a process of superficial adsorption as described by a Langmuir isotherm. The mathematical expression resulting from this combination is an expanded Avrami equation dependent on the antimalarial medicine concentration, and the kinetic constant of the adsorption process. In a later work, Fitzroy et al.[26] improved this equation by adding a parameter related with the maximal yield of β-hematin formed in the absence of the antimalarial compound. Pasternack et al.[19] proposed

an equation that consists of a linear combination of the first order and the Avrami equations, suggesting the underlying effects of both hemin concentration and crystal random nucleation and growth in the medium. Egan and Tshivhase[27] proposed a modification of the Gompertz equation to fit the kinetics of crystallization of β-hematin in an aqueous medium in the presence of benzoic acid. Gompertz equation is an empirical model that has been used for the description of biological phenomena such as the growth of tumors, although in the last 30 years it has been used for modeling the crystallization of fats and oils. Olafson et al.[28] used time-resolved in situ atomic force microscopy to investigate the mechanisms of β-hematin crystallization and inhibition by chloroquine and reported that the crystallization process follows a classical layer-by-layer mechanism in which new layers are generated by two-dimensional nucleation and the crystal grows by the attachment of molecules from the solution. The authors did not propose an equation for modeling this kinetic mechanism, however from the reported results it is possible that the Avrami model could explain the results. Rifaie-Graham et al.[29] studied the kinetics of β-hematin crystallization by using depolarized light scattering. The authors reported that the formation of β-hematin follows a process of nucleation and growth, in which initially small clusters form until a seed of specific critical size is reached, then the growth occurs.

From this recompilation of quantitative and qualitative proposals, it seems that the Avrami model should be the model of choice. However, we noticed several attempts to modify this equation, either by explicitly incorporating the effects of the antimalarials or by combining it with other kinetic equations. It is evident that we do not fully understand the kinetics of formation and inhibition of the β-hematin crystals in the absence and in the presence of

antimalarials. More work is needed in this area, and a comparative approach between different models could yield a better description of the experimental data. We are aware that the kinetic data alone is not able to distinguish between different possible mechanisms of formation and inhibition. Complementary studies should be included, and a plausible alternative is to use quantitative characterization of different physico-chemical properties exhibited by the β-hematin crystals. Here, it is worth mentioning that Ali and Oppeneer[30] reported that a detailed knowledge of the crystal and electronic structures as well as magnetic, vibrational and optical properties of the hemozoin crystals, and therefore, the β-hematin crystals, is crucial for the design of antimalarial medicines and malarial diagnosis. Furthermore, variations in morphology, intensities of the X-ray diffraction crystallographic planes, unit cell parameters, positions and intensities of the infrared spectroscopic signals could be related with the mechanisms of crystallization and inhibition of the β-hematin crystals.

In this paper we investigate the kinetics of β-hematin crystallization from hemin in aqueous medium containing varying concentrations of antimalarial chloroquine. The experimental kinetic data is fitted to eleven model equations. This kinetic study is complemented by quantitative characterization of the morphology by scanning electron microscopy, crystallographic structure by powder X-ray diffraction (PXRD) using Rietveld method and vibrational spectra by infrared spectroscopy. We used Density Functional Theory calculations to understand the IR spectra of the samples.

MATERIALS AND METHODS

Synthesis of β-hematin from hemin with and without chloroquine

Hemin chloride from bovine (≥ 90% purity) and chloroquine diphosphate salt (>98% purity) were acquired from Sigma-Aldrich. Analytical grade Pyridine was supplied by Supelco Inc. (Sigma-Aldrich). Acetic acid 100% anhydrous and sodium hydroxide analytical pellets were purchased from Merck. 50 mL sterile erlenmeyers were employed as reaction vials in the β-hematin synthesis processes. A heating plate with a thermocouple was used for temperature control during the synthesis. Centrifugation was carried out in a LABNET Z100.

The method of synthesis, with some modifications, is based on the one reported by Egan et al.[8] Initially, solutions of glacial acetic acid at pH 1,7 were prepared. For that purpose, 10 mL of acetic acid were added to 40 mL of distilled water. In each synthesis, 80 mg of bovine hemin chloride was used. Hemin was dissolved in 40 ml of 0,4 M NaOH solution. This solution was prepared by adding 795 mg of NaOH to 50 mL of distilled water. The mixture was stirred in a range between 100 and 130 rpm for 30 minutes. Subsequently, the temperature is raised to 60°C and 10 mL of the previously prepared solution of acetic acid was added; the mixing of acetic acid solution and basic hemin results in the formation of an acetate buffer at pH 4,75. The final concentration of the hemin chloride solution was 2,45 mM.

The temperature of the solution was maintained for 4 hours, but agitation is applied only during five minutes every half-hour.

After 4 hours of synthesis at 60°C, the heating magnetic stirrer was turned off and the solution was allowed to stand for one hour, a time in which the β-hematin precipitates completely in the solution. The precipitated material was vacuum filtered with alternate washings: five times with 5 mL of distilled water and five times with 5 mL of ethanol. The obtained solid was dried in the oven at 37°C for 48 h.

The synthesis of β-hematin in presence of chloroquine was performed similarly as described above, the only difference is that chloroquine is dissolved in acetic acid solution at concentrations of 0,565 mM and 1,667 mM before mixing with NaOH solution. The chloroquine solutions in acetic acid were obtained by adding 10 mg and 35 mg, respectively, of chloroquine diphosphate in 10 mL of acetic acid solution previously prepared.

Kinetics of formation of β-hematin.

We adapt the colorimetric assay developed by Ncokazi and Egan[31] to determine the kinetics of β-hematin formation. For that purpose, aliquots of the reaction medium are taken every 30 minutes. The samples are deposited in vials where water and 5% pyridine are added. The mixture was vortexed for 60 seconds to ensure that the pyridine forms a complex with the hemin present in the medium. At this point, all the hemin that has not been converted to β-hematin is converted to soluble hemin. The mixture is then centrifuged for 10 minutes at 4000 rpm to separate the β-hematin that precipitates at the bottom of the vial. The supernatant is analyzed spectrophotometrically (λ_{max} at 405 nm) for detecting the presence

of hemin as a pyridine adduct (see Figure 1). The data obtained can be represented spectrophotometrically as the percentage of hemin converted to β-hematin (% conversion) versus reaction time. The spectral measurements were performed on a Genesys 10 UV-Vis spectrophotometer.

FIGURE 1

Table 1 shows the equations of the different kinetic models used to fit the experimental kinetic curves. In the equations, *y* represents the total % conversion of hemin to β-hematin at time, *t*. This conversion was calculated from absorbance measurements at 405 nm for the dipyridine hemin complex. The parameter y_0 is related to the final (or in some cases, the initial) absorbance at 405 nm. The parameters y_1 and y_2 are the contributions to the conversion of hemin to β-hematin from the different equations. z_0 is the observed rate constant in the absence of antimalarials. The k_i parameters, with i = 0, 1, 2 and A, are the kinetic constants for the different models. K_{ads} is the adsorption equilibrium constant. The parameter n is related to the order of the reaction. Y is the maximal yield of β-hematin formed in the absence of antimalarial medicine. [Q] is the concentration of antimalarials. μ and λ are descriptive and empirical parameters that do not provide direct insight into the microscopic mechanism.

Regarding the Avrami equation, it explains crystallization as the result of nucleation and growth processes. In this equation, n is taken as an integer in the range between 1 and 4, and it represents the number of (n -1) dimensions in which the crystals grow and the nucleation itself. It is noticed that as n goes from 1 to 4, the shape of the curve changes from hyperbolic to sigmoidal. The z constant complements the information and allows

relating the growth of the crystal with the density of reactants and products. This type of crystallization is favored by the presence of “molecular seeds” that act as nuclei for the formation of a crystal.

More details about the meanings of these parameters can be found in the original references listed in the last column of Table 1.

TABLE 1

The test of goodness of fit was studied by using the three equations listed in Table 2.

TABLE 2

Analysis of the kinetic data was carried out using programs written in Python. For that purpose we used the numpy, matplotlib.pyplot, panda and scipy libraries. We used the non-linear least-squares fitting methods as implemented in the optimize.curve_fit function of the scipy library.

Characterization techniques

FTIR analyses were performed at room temperature on a IRTracer-100 infrared equipment (Shimadzu, Japan) using 64 scans, 4,0 cm^{-1} resolution and a wavenumber range between 4000 and 400 cm^{-1}. The positions and intensities of the IR bands in each FTIR spectra were determined using the Voigt peak fit type of analysis as implemented in the RECOIL software.[32] It was also used in the analysis of IR spectra, for which their bands can exhibit the Voigt shape.

The PXRD diffraction data were collected using a Panalytical diffractometer X'Pert PRO MPD with a Cu-Kα X-ray source. The measurements were performed in 2θ range from 10° to 80° using steps of 0,04° and time per step of 23 s. The quantitative analysis of the PXRD patterns for all samples was carried out using the MAUD program, which combines the Rietveld method and the Fourier transform analysis.[33] The analysis was done in the 2θ range from 10° to 40°, because above 40° no diffraction peaks were noticeably observed. The structural model used was reported by Pagola et al.[34] The *a*, *b* and *c* unit cell lengths; the α, β, and γ unit cell angles; and average crystallite sizes of the sample were refined. The average crystallite size and the texture were assumed to be isotropic and arbitrary respectively. The following instrumental factors were also considered in the refinement: incident intensity, four-order polynomial background and the three full widths at half maximum of the line profile included in the Caglioti formula for the instrumental broadening.

The SEM micrographs were obtained using a JEOL JSM-6490LV scanning electron microscope with magnifications of 200X, 5000x, 20000x, 30000x and 40000x. The average crystal sizes of the β-hematin crystals were determined using the Image J software. For that purpose, 20 crystals were taken from the SEM micrographs for each sample and their heights and widths were averaged.

Simulation methods

Energy calculations and structure optimizations for the model were performed using the real-space finite-difference Density Functional Theory code GPAW.[35] Exchange and correlation functional used was the Perdew, Burke, and Ernzerhof (PBE)[36] with TS09 correction.[37] The Kohn-Sham wave functions were expanded directly on a real space grid with a grid spacing of 0,2 Å. Optimizations of the considered structures were performed until the maximal force was below 0,01 eV/Å on any atom. The vibrational modes were calculated from a finite difference approximation of the dynamical matrix and the IR intensities from a finite difference approximation of the gradient of the dipole moment.[38]

RESULTS

Kinetics of β-hematin crystallization

Figures 2 to 4 show the results of the analysis of the kinetics of β-hematin crystallization in absence and in presence of chloroquine. Table 3 shows the statistical parameters from the fits.

FIGURE 2

FIGURE 3

FIGURE 4

TABLE 3

In the case of β-hematin, and based on the R^2, RMSE and MAPE values (see Table 3), the order of the models, from the most appropriate to the less appropriate fit, is as follows: Second order + Logistic > Order 1 and Avrami > Logistic > Modified Gompertz > Avrami > Modified Avrami > Order 1 ≈ Avrami and Langmuir I ≈ Avrami and Langmuir II > Second order > Order 0. In the case of β-hematin with Cq 0,565 mM the order of the models is: Order 1 and Avrami> Second order + Logistic > Modified Gompertz > Avrami > Logistic > Second Order > Order 1 ≈ Avrami and Langmuir I ≈ Avrami and Langmuir II > Modified Avrami > Order 0. In the case of β-hematin with Cq 1,667 mM the order of the models is: Order 1 and Avrami ≈ Second order + Logistic > Second order > Avrami > Modified Gompertz > Order 1 ≈ Avrami and Langmuir I ≈ Avrami and Langmuir II > Logistic > Modified Avrami > Order 0. In general, from the statistical analysis, it is evident that the linear combination of Order 1 and Avrami models and the linear combination of Second order and Logistic models reproduce better the kinetic experimental data for all β-hematin crystals in absence and in presence of chloroquine. The less appropriate model is the zero order.

Tables 4-1 and 4-2, list some of the parameters obtained by fitting the kinetic curves of all samples with the equation that linearly combines Order 1 and Avrami models and Second order and Logistic models, respectively. It is noticed that the yield, or formation, of β-hematin (see parameter y_0) is inhibited by the presence of chloroquine. Furthermore, as the chloroquine increases, the kinetic constant related to the Order 1 part of the equation increases, while the kinetic constant of the Avrami part decreases. These results mean that both the rate of formation of the β-hematin crystals from hemin concentration and also the

rate of nucleation and growth of the β-hematin crystals are affected by the presence of chloroquine.

TABLE 4-1

TABLE 4-2

Analysis of ANOVA in Figure 5, shows two different variables that exhibit a representative difference in β-hematin percentage conversion when there are different chloroquine concentrations. This analysis was done using GraphPadPrism 5 software. Comparison between 0,565 mM and 1,667 mM of chloroquine and the sample without antimalarial drug, present a good parameter p with value of 0,0004. It is clear that the percentage of conversion of hemin to β-hematin is reduced by chloroquine.

FIGURE 5

PXRD results

Figures 6, 7 and 8 show the experimental and the calculated PXRD patterns of the samples prepared in absence and in presence of two different concentrations of chloroquine. The Miller indices of some representative crystallographic planes of β-hematin are also indicated in the figures. It is noticed that the calculated PXRD patterns reasonably follow the experimental data, indicating that the samples synthesized in the present work consist of only β-hematin. No other compound was detected by PXRD.

FIGURE 6

FIGURE 7

FIGURE 8

The triclinic unit cell parameters derived from the fittings of the patterns using the MAUD program[32] are reported in Table 5. It is noticed that the cell parameters are quite similar for all samples, indicating that the presence of chloroquine has no appreciable effect on the values. Moreover, these values are also similar to the cell parameters reported by Pagola et al.[34]

TABLE 5

By careful visual inspection of the PXRD patterns for all samples, it is possible to notice variations in the relative intensities as well as the relative peak broadenings in some Bragg reflections as the chloroquine content in the samples increases. To quantify these variations, we determined both the areas and the full-width at half maximum (FWHM) of the five most intense and well-resolved Bragg peaks for each PXRD pattern. To justify this analysis, we have taken into consideration these three aspects: (1) according to Buller et al.[39] Weissbuch and Leiserowitz[2] the most manifested faces of the β-hematin crystals are the {100} and {010}, the less developed {011}, and the minor {001} and therefore these are the crystal faces that are more exposed to the antimalarial drugs, *i.e.* these are the preferable faces for chloroquine binding; (2) on the contrary, the crystallographic planes with Miller indices of (131) and (031) are not similarly exposed to the drugs, *i.e.* it is expected that the Bragg reflections associated these planes should not be so much altered due the presence of the drugs; and (3) in the experimental PXRD patterns of all samples, the Bragg peaks

associated to the (100), (001), (020), (131) and (031) crystallographic planes are well-resolved, intense and isolated, *i.e.* these peaks do not overlap with other Bragg peaks.

Here it is worth mentioning that Solomonov et al.[40] determined the FWHM for different Bragg reflections and from these values, by using the Scherrer formula, they determined the relative change of the crystal coherence length along the c-axis, L{001}, relative to the coherence lengths along different crystallographic directions L{hkl}, including {031} and {131}. The authors assumed that if the quinoline is adsorbed and occluded via the {001} or {011} face, then it should result in broader {001} or {011} X-ray reflections relative to the other {hkl} reflections than those of the pure samples. However, they did not observe a decrease in L_{001}/L_{hkl} for β-hematin crystals grown in MeOH-DMSO medium, although they reported a marginally positive effect for β-hematin crystals grown in $CHCl_3$ medium. Additionally, Dilanian et al.[41] investigated the changes in the intensity ratios of some selected Bragg reflections, I_{020}/I_{001}, I_{131}/I_{013}, I_{031}/I_{001} and I_{131}/I_{001}, to detect changes in the microcrystalline structure of β-hematin. The authors analyzed nanoscale crystals of β-hematin and found significant differences in β-hematin data collected during serial femtosecond nanocrystallography and synchrotron crystallography experiments. They suggested that structural differences between the nanocrystal and larger crystalline forms of β-hematin are the most plausible explanation for the observed differences.

Based on these two works, therefore, we have performed a similar analysis and made a comparison of the intensities and the peaks broadening of the most affected Bragg

reflections ((001), and (100)) with respect to the less affected ones ((131), (031) and (020)). The results of these analyses are reported in Tables 6 and 7.

TABLE 6

TABLE 7

Regarding the intensity ratios, it is noted that $I_{001/031}$ and $I_{100/031}$ tend to decrease with increasing chloroquine concentration. On the contrary, the intensity ratios for the other planes do not show regular variations. On the other hand, it is noted that $L_{100/031}$ and $L_{100/131}$ tend to increase with increasing chloroquine concentration. On the contrary, the $L_{001/hkl}$ ratios do not show regular variations. We did not observe a decrease in L_{001}/L_{hkl} for β-hematin with increasing chloroquine concentration. These results are very similar to ones reported by Solomonov et al.[40] who did not find a decrease in L_{001}/L_{hkl} for β-hematin crystals grown in MeOH-DMSO medium. These results may suggest that the morphologies of the β-hematin crystals are affected by the presence of chloroquine, however not all the crystallographic planes are affected similarly.

Finally, we would like to mention that despite the fact the collection of the PXRD patterns for all samples were performed under identical experimental and instrumental conditions, the number of counts (*i.e.* the values of intensities in the vertical axis) per angle are greatly reduced as the chloroquine content increases. For example, the number of counts for the most intense Bragg reflection (the (131) peak), is reduced by about 40 % and 60 % for β-hematin plus 0,565 mM chloroquine and β-hematin plus 1,667 mM chloroquine in comparison to the sample without chloroquine. This result could be an indirect indication

of lowering of the crystallinity of the samples as chloroquine increases. These results are in good agreement with our SEM results shown below.

Here, it is worth mentioning that Straasø et al.[42,43] and Marom et al.[44] proposed the existence of two phases in β-hematin: one major phase, that it is the one published by Pagola et al.[34] and a minor phase that has been reported in few studies. The authors explain that this is due to the formation of four stereoisomeric heme dimers of Fe^{3+}-PPIX: two centrosymmetric, called cd$\bar{1}_1$ and cd$\bar{1}_2$, and two enantiomeric, called cd2(+) and cd2(−). The following five Bragg peaks are indicative of the presence of this minor second phase, composed of the centrosymmetric cd$\bar{1}\bar{2}$ stereoisomer, in the PXRD pattern of β-hematin (see the blue peaks shown in Figure 4 of paper by Straasø et al.[42] and in Figure 5 of paper by Straasø et al.[43]): (i) a shoulder at lower angle side of (100) peak; (ii) a peak between ($\underline{1}10$) and (110) peaks; (iii) a peak between (001) and (020) peaks; (iv) a peak between (031) and (131) peaks and (v) a peak at higher angle side of (131) peak. Therefore, we first tried simple visual inspection to check for the existence of these five peaks in the PXRD patterns of our samples. However, we could see none of them. As a second check, we fitted again the PXRD patterns of all samples by introducing the major and minor β-hematin phases with the unit cell dimensions published in Table 2 of the paper by Straasø et al.[43] We could not see any improvement in the PXRD analysis. Because we did not observe the centrosymmetric cd$\bar{1}\bar{2}$ stereoisomer, our results suggest that our β-hematin crystals are mainly composed of centrosymmetric cd$\bar{1}1$ and enantiomeric cd2(+) stereoisomers. The minor phase of β-hematin has been reported in a few studies, probably suggesting that its

formation is very dependent on the synthesis procedure, for example, temperature, reactive types and concentrations, pH etc.

IR results

To quantitatively analyze the FTIR spectra for the three samples investigated in the present work, we fitted each spectral band using the Voigt function as implemented in the RECOIL software.[32] This type of analysis was based on the reports that the spectral line shapes can be described by Voigt function.[45,46] The fitting of the complete FTIR spectrum from 400 to 4000 cm^{-1} is somewhat difficult, because of the large number of bands. In order to simplify the analysis, we decided to divide the spectrum into three regions: 400-1000 cm^{-1}, 1000-2000 cm^{-1}, and 2000-4000 cm^{-1}. Figure 9 shows the experimental and the fitted FTIR spectrum in the three regions for β-hematin prepared in absence of chloroquine. Similar analyses were performed for the other samples. It is noticed that the calculated curve reasonably follows the experimental FTIR data.

FIGURE 9

The left sides of Figures 10, 11 and 12 compare the FTIR spectra of the three samples in the three mentioned regions. The right sides of Figures 10, 11 and 12 show the relative areas versus the positions for some selected IR bands. The areas were obtained by means of the Voigt analysis of the IR bands, and the relative areas were determined with respect to

the most intense band registered in each region. In this order of ideas, it is pointed out that the region that presents less change in the relative areas is between 0 and 1000 cm^{-1}. However, in the regions of 1000-2000 cm^{-1} and 2000-4000 cm^{-1} some variations are observed, suggesting that the effect of the chloroquine on β-hematin is better detected in this region.

FIGURE 10

FIGURE 11

FIGURE 12

Table 8 shows the positions and the relative intensities of some selected infrared bands as obtained from the fitting procedure. The intensities for the bands in the 1000-2000 cm^{-1} region are relative to the intensity of the 1206 cm^{-1} band, while in the 2000-4000 cm^{-1} region are with respect to the 2850 cm^{-1} band.

TABLE 7

In the 1000-2000 cm^{-1} region, the most intense bands characteristic of β-hematin are seen in the vicinity of 1663 and 1210 cm^{-1}. The former peak is believed to arise from the C=O stretch of the carboxylate group coordinated to the Fe(III) center, while the latter arises from the C-O single bond stretch of the same group[30]. We selected the peak at 1210 cm^{-1} as the most convenient for quantitative monitoring of the reaction because there is less overlap with neighboring peaks. In the 2000-4000 cm^{-1} region, three intense bands with positions at 3299, 2917 and 2850 cm^{-1} are observed, which are assigned to the presence of amine

groups with stretching type vibrations. Something important to note is that the band at 2850 cm^{-1} disappears completely when adding both concentrations of chloroquine. On the other hand, in the 1000-2000 cm^{-1} region, there are three intense bands with positions at 1711, 1661 and 1206 cm^{-1}, which are identified with the presence of carboxyl groups with stretching type vibrations. These bands are identified in the unit cell as corresponding to the union between dimers through hydrogen bridges, union between porphyrin rings and the Fe-O-C bond, respectively.[30] Finally, in the region of 400-1000 cm^{-1}, no changes in the positions of the IR bands are perceived as the concentration of chloroquine increases.

IR simulation results

We model the β-hematin crystal with an isolated hemin dimer. In this work, we use Density Functional Theory calculations as implemented in GPAW code[35] with the exchange-correlation functional PBE[36] with vdW correction TS09[37] that can be used to examine differences of energies rather than absolute ones. We can simulate the main changes in IR when the dimerization of hemin takes place. Results are summarized in Table 8 and Figure 13.

TABLE 8

FIGURE 13

There is an important characteristic peak at 1207 cm^{-1} assigned to esters stretching in Fe-O-C bonds. In simulation, this peak is found at 1165 and 1171 cm^{-1} with an underestimation of about 45 cm^{-1}. Once the dimerization takes place, there is also a double peak formation seen in the IR experimental spectra at 1661 and 1710 cm^{-1}. The peak at 1661 cm^{-1} which is assigned to carboxyl bonded to central Fe stretching appears in the simulation at 1643 and 1646 cm^{-1} with an underestimation of about 20 cm^{-1}, consistent with the underestimation of the 1207 cm^{-1} peak. There is then the vibration at 1710 cm^{-1} in the experiment which is carboxyl that is hydrogen-bonded to the other dimer in the crystal stretching. The simulated peak is found at 1764 cm^{-1} and 1766 cm^{-1} with overestimation of about 50 cm^{-1}. A failure we ascribe to the model which consists of a single dimer. Reference calculations[30] also found a significant overestimation of the same peak, obtaining it at 1825 cm^{-1} with B3LYP functional and suggesting the same origin for the overestimation.

The region above 2800 cm^{-1} is of high interest because the experimental IR suffers dramatic changes upon complexation with the antimalarial chloroquine. In the simulated IR spectra, the higher excitation region is found to be overestimated, which could be again related to the interaction with neighboring dimers inside the crystal that we do not describe in our model. In this case, however, we can analyze the vibrational trajectories at this energy range and propose possible regions of interaction with the chloroquine. The highest energy peak in the experiment is assigned to the OH vibration is also the highest in energy vibration in the simulation, as is observed in the vibrational trajectories. The OH peak disappears in the experimental β-hematin IR spectrum in presence of chloroquine. The region just below, in

the range 2900-3200 cm^{-1} corresponds in the simulation to C-H vibrations of mostly methyls and some vinyls which become suppressed after the interaction. In summary, the proposed sites for chloroquine β-hematin interaction are hydrogens present in the terminal COOH groups, methyls and vinyls. Such sites agree with the previously proposed interaction sites[39] and in agreement with PXRD results in this work.

SEM Results

Figures 14, 15 and 16 show the SEM micrographs of β-hematin, β-hematin prepared in presence of 0,565 mM chloroquine, and β-hematin synthesized in presence of 1,667 mM chloroquine, respectively. The sample without antimalarials shows crystals with regular shapes and sizes. The shapes are of needle-like type morphologies, *i.e.*, parallelepipeds of about 760 nm long and 140 nm wide. However, when formed in the presence of chloroquine, the crystals are organized in crystal twinning with inhomogeneous distributions, exhibit lower crystal sizes and are symmetrically tapered at the ends of the needles, as if having spines-like morphologies. The spine-like habit was previously observed by Solomonov and co-workers[40] in β-hematin crystals formed in another reactive medium (MeOH-DMSO solution containing hemin and 2,6-lutidine base) containing 10% chloroquine (mol/mol hemin). The authors explained that the spine-like habit is due to stereoselective additive binding of chloroquine to {001} or {011} ledges, and they used a model of stepped face morphology for showing it.

FIGURE 14

FIGURE 15

FIGURE 16

Table 9 shows the average heights and widths of the crystals calculated from the SEM micrographs for all samples. It is observed that with the increase of the antimalarial, the sizes of the crystals decrease, this change being greater for the sample with the highest chloroquine concentration. Furthermore, the height to width ratio of the crystals changes with the presence of chloroquine. In general, it is evident that the presence of chloroquine drastically affects the morphology of the β-hematin crystals: induces the formation of crystal twinning with non-homogenous distribution, reduces the crystal sizes, produces crystals with different height to width ratio, and the crystals are symmetrically tapered at the ends like with spine-like morphology.

TABLE 9

DISCUSSION

One of the great challenges of researching in malaria is to completely understand how hemozoin is formed and how this crystallization process can be inhibited. Most studies support the formation of lipid mediated nucleation, and it is now widely accepted that this happens at the inner membrane lipid surface of the parasitic digestive vacuole.[4,10,20]

However, there are other reports suggesting that hemoglobin degradation and hemozoin crystals formation can occur in compartments outside the digestive vacuole,[47,48] which could imply the formation in the absence of lipid catalysts. Therefore, the formation mechanisms should be explored in different mediums.

The effort to describe the experimental data has led to the implementation of different models for kinetic crystallization. Starting with zero order kinetic model, simple first order kinetic model, Avrami, second order kinetics, Logistic, linear combinations of some of these models (Order 1 + Avrami, Second order + Logistic), modifications to the rate constants in existing models to explicitly include the presence of the antimalarials (e.g. modified Avrami), complex combination of existing models (e.g. Avrami and Langmuir) and empirical models (e.g. Gompertz).

In this work, we applied these equations to understand the formation of β-hematin crystals from hemin in aqueous-acetate medium and in the presence of chloroquine. As the different statistical parameters showed (Table 3), the best correlations with experimental data in the three concentrations used were achieved by using the model proposed by Pasternack et al., *i.e.* Order 1 + Avrami,[19] and the kinetic model proposed in this work, *i.e.* Second order + Logistic. Let us discuss each model separately. Pasternack and co-workers reported that the reason to use the Order 1 + Avrami model is that the kinetic data are biphasic, in which the primary change is quite rapid and is represented by the Avrami exponential, whereas the second change is slower and smaller, represented by the Order 1 exponential. In fact, the authors reported for β-hematin prepared in 1-hexanol that kA= 0,14 min^{-1}, and k1= 0,0054 min^{-1}; in carbon tetrachloride that kA= 0,012 min^{-1}; etc. In contrast, our values are different

from those reported by Pasternack et al.[19] and this is because we used a different medium to prepare our samples. In aqueous-acetate we found that kA= 0,007 min^{-1}, and k1= 0,016 min^{-1}. Therefore, we suggest a different interpretation to the one made by Pasternack et al.[19] given the biphasic nature of the kinetic, instead of fast and slow changes ascribed to the exponentials, we could think of them as heme availability and nucleation and growth. This interpretation is inspired by the recently proposed assembly-line model for heme detoxification by heme crystallization[4] which links the rate of hemoglobin degradation in the digestive vacuole and heme crystallization (see Figure 6 in the paper by Kapishnikov et al.[4]). Of course, in our experiments, we do not have the same medium as the digestive vacuole, nor do we have hemoglobin degradation, but we have hemin availability and nucleation and growth.

We propose that the Order 1 kinetics depends upon the reactive precursor concentration and the Avrami exponent with nucleation and growth of the crystals. To make our case for this interpretation of the Order 1 model, we have to consider that the dependence on the concentration of β-hematin formation is due to the nature of the crystallization units, which are the π-π dimers or the μ-propionate dimers; hence, when the concentration of dimers increases, the concentration of crystal units rises, allowing the formation and growth of more crystals per volume of the medium. Now, for the Avrami model, using the literature reports previously evaluated, we can propose the route of formation of β-hematin crystals in our experiments as a process of crystallization of hemin through dimerization and self-assembly into β-hematin. In detail, the process can be as follows: the aqueous medium contains mainly π-π dimers, which can either remain or transform into μ-propionate

dimers, mostly of the centrosymmetric cd$1\bar{1}$ type. The dimers either bind to existing β-hematin crystals or form new crystals through heterogeneous (a fractal type) nucleation.

A similar behavior was observed in the kinetic model proposed in this work (Second order + Logistic), in which the biphasic nature of the data was also observed in the three concentrations used, here it is interesting to point out that this is a model based on the assumption that in the solution we have π-π dimers as suggested by De Villiers et al.[49] and then the dimers interlink via the propionate group as suggested by Klonis and colleagues.[50,52] We ascribe our suggested interpretation to the Pasternack's[19] biphasic model for this one too, in which one term (second order) could be interpreted as dimeric hematin availability and the second term (Logistic) to nucleation and growth.

Let us justify in more detail the use of the second order and logistic models. According to de Villiers et al.[49] in aqueous solution, the π-π dimers are the main reactive species. Although, it could also happen that monomers are also present.[54]

In the aqueous-acetate medium, and regarding only the π-π dimers, three things can occur: (i) π-π dimers transform into μ-propionate dimers, without splitting into monomers. The computational simulations by Egan et al.[22] have shown that to transform the π-π dimers into μ-propionate dimers in lipids require only bonding of the propionate groups to Fe(III) and release of H_2O. de Viiliers et al.[49] also suggested this can occur in aqueous medium. We will assume that in aqueous-acetate medium this could also be happening; (ii) π-π dimers splits into two monomers, and then two monomers form μ -propionate dimers; and (iii) π-π dimers remains, *i.e.* neither transformation nor splitting occur.[50,52]

Therefore, in our aqueous-acetate medium, π-π dimers or μ-propionate dimers could be the main reactive precursors from which nucleation and growth proceeds to form the β-hematin crystals. ¿How to model the kinetics of β-hematin crystallization for these two possible reactive precursors? We are going to propose a kinetic model for i) and iii).

i) If dimers are the reactive precursors, then it could be expected that the reaction follows the second order kinetics, because 2 dimers → 2 dimers linked via H-bonding or π-bonding or P-bonding.[50,52] The rate (dy/dt) of this reaction would likely be $dy/dt = -k_2(y_1 - y)^2$, in which y = [product] and k_2 is the second order rate constant. Such tetramer aggregate also via H-bonding, π-bonding or P-bonding to other μ-propionate dimers until a critical nucleus size is reached, from which the crystal grows. The second order kinetic equation, written in terms of the concentration of the product, *y*, *i.e.* the concentration of β-hematin, at a given time *t*, is: $y = y_1 - \frac{1}{k_2 t + c_2}$. Here $y1$ is the final β-hematin concentration, k_2 is the second order rate constant and c_2 is the integration constant. Note that the precursor, x, and the product, y, concentrations are related by: $x/x_1 = 1 - y/y_1$, in which x_1 and y_1 are the initial precursor and final product concentrations, respectively.

iii) If π-π dimers are the reactive precursors, then it could be expected that the reaction follows the second order and we propose a second term that corresponds to nucleation and growth following a logistic model. In the nucleation model, the presence of an amount of already crystallized dimers y acts as seed capturing more dimers into crystallization which has the form of a logistic model. It corresponds to the following process: the π-π dimers

assemble into columnar aggregates via P bonding first and then form sheets via propionate linkage to other π-π dimers. Finally, sheets may aggregate by H-bonding.[50,52] The logistic equation is of the form dy/dt= k_n *y (y0 - y). The solutions to the second order kinetic equation and the logistic equations combined together into one kinetic equation, written in terms of the concentration of the product, y, *i.e.* the concentration of β-hematin, at a given time t, are: $y = \frac{c_1 y_0 \ exp(y_0 k_1 t)}{1 + c_1 \ exp(y_0 k_1 t)} + y_1 - \frac{1}{k_2 t + c_2}$. As already mentioned, we fitted the model and the result is competitive with our previous best fitting model (order 1 and Avrami).

Finally, let us discuss the inhibition of β-hematin crystals by chloroquine. We have found that the increment in the chloroquine concentration decreases the yield of β-hematin, reduces the crystal sizes, modify the Order 1 and Avrami rate constants and favors the formation of crystal twinning. Here, it is worth mentioning that Kapishnikov and colleagues[4] used their recently proposed assembly-line model for heme detoxification by heme crystallization to explain the boot-like shape of some hemozoin crystals, reported in a rodent malaria parasite by Matz et al.[51] as excessive directional branching, due to uncontrolled hemozoin precipitation. Of course, we must adapt this model to our situation. Therefore, it is suggested that the coupling between the rate of hemin availability and the rate of hemin dimerization and crystallization is altered by the presence of chloroquine, which changes these two rates. This is perhaps evidenced by the observed variations in the rate constants of the Order 1 and Avrami exponents. Now, on the other hand, we also found from PXRD, that the intensities of the (100) peak relative to the (131) peak increased with increasing chloroquine concentration. This result is in good agreement with those reported

by Olafson et al.[28] in which chloroquine inhibits β-hematin crystallization by binding to molecularly flat {100} surfaces. We propose a mechanism of action of chloroquine that considers both inhibition of the formation of crystals by binding to some crystallographic surfaces and also changes the availability of hemin, which is necessary for nucleation and growth of crystals.

CONCLUSIONS AND PERSPECTIVES

We studied the kinetics of formation of β-hematin crystals when these are synthesized from hemin in aqueous-acetate medium in the absence and in the presence of 0,565 mM and 1,667 mM chloroquine antimalarials. To understand the kinetics, we fitted the experimental data with eleven different equations and found that the models that better describe all curves are the linear combinations of order 1 + Avrami equations and second order + logistic equations. We propose that the biphasic nature of the kinetic curves are due to both the hemin dimer availability and the β-hematin nucleation and growth. It is also observed that as the concentration of antimalarial increases, the percentage of conversion of hemin to β-hematin decreases, the Avrami kinetic constant tends to decrease and the order 1, second order and logistic kinetic constants increase. The Rietveld analysis of the PXRD pattern indicates that the synthesis of β-hematin was successful. It was found that the presence of chloroquine did not affect the unit cell volume. However, it changed the PXRD intensities and broadenings of some crystallographic planes. Through IR spectroscopy, the formation of the dimers was corroborated, making a follow-up of the corresponding bands of each functional group that indicates the formation of new bonds between hemin molecules. The

β-hematin crystals exhibit needle-like type morphologies with lengths and widths of the order of 760 nm and 140 nm, respectively. The presence of chloroquine drastically changes these morphologies, reducing the crystal sizes, inducing the formation of crystal twinning and needles with symmetrical tapered ends. In order to have a more complete picture of the β-hematin formation, a study should include the kinetics of crystallization in more mediums and with different antimalarials, but this is the purpose of a future work.

CONFLICT OF INTERESTS

There are no conflicts to declare.

ACKNOWLEDGEMENTS

We greatly acknowledge the financial support from CODI-Universidad de Antioquia through the projects ("Convocatoria Programática 2019-2020: Ciencias Exactas y Naturales", Project code 2020-33176 and "Estrategia de Sostenibilidad del Grupo de Estado Sólido 2020-2021").

REFERENCES

(1) World Health Organization. *World Malaria Report 2021*; Geneva, **2021**. ISBN 978-92-4-004049-6

(2) Weissbuch, I.; Leiserowitz, L. Interplay between Malaria, Crystalline Hemozoin Formation, and Antimalarial Drug Action and Design. *Chemical Reviews*. November **2008**, pp 4899–4914. https://doi.org/10.1021/cr078274t.

(3) Dalapati, T.; Moore, J. M. Hemozoin: A Complex Molecule with Complex Activities. *Curr Clin Microbiol Rep* **2021**, *8*, 87–102. https://doi.org/10.1007/s40588-021-00166-8/Published.

(4) Kapishnikov, S.; Hempelmann, E.; Elbaum, M.; Als-Nielsen, J.; Leiserowitz, L. Malaria Pigment Crystals: The Achilles′ Heel of the Malaria Parasite. *ChemMedChem*. John Wiley and Sons Ltd May 18, **2021**, pp 1515–1532. https://doi.org/10.1002/cmdc.202000895.

(5) Egan, T. J.; Ross, D. C.; Adams, P. A. Quinoline Anti-Malarial Drugs Inhibit Spontaneous Formation of β-Haematin (Malaria Pigment). *FEBS Lett* **1994**, *352* (1), 54–57. https://doi.org/10.1016/0014-5793(94)00921-X.

(6) Egan, T. J.; Hempelmann, E.; Mavuso, W. W. Characterisation of Synthetic β-Haematin and Effects of the Antimalarial Drugs Quinidine, Halofantrine, Desbutylhalofantrine and Mefloquine on Its Formation. *J Inorg Biochem* **1999**, *73*, 101.

(7) Blauer, G.; Akkawi, M. On the Preparation of β-Haematin. *Biochem. J* **2000**, *346*, 249–250.

(8) Egan, T. J.; Mavuso, W. W.; Ncokazi, K. K. The Mechanism of β-Hematin Formation in Acetate Solution. Parallels between Hemozoin Formation and Biomineralization Processes. *Biochemistry* **2001**, *40* (1), 204–213. https://doi.org/10.1021/bi0013501.

(9) Bohle S; Helms J. Synthesis of β-Hematin by Dehydrohalogenation of Hemin. *Biochem Biophys Res Commun* **1993**, *193* (2), 504–508.

(10) Fitch, C. D.; Cai, G.-Z.; Chen, Y.-F.; Shoemaker, J. D. Involvement of Lipids in Ferriprotoporphyrin IX Polymerization in Malaria. *Biochim Biophys Acta* **1999**, *1454*, 31–37.

(11) Hoang, A. N.; Ncokazi, K. K.; De Villiers, K. A.; Wright, D. W.; Egan, T. J. Crystallization of Synthetic Haemozoin (β-Haematin) Nucleated at the Surface of Lipid Particles. *Dalton Transactions* **2010**, *39* (5), 1235–1244. https://doi.org/10.1039/b914359a.

(12) Pisciotta, J. M.; Coppens, I.; Tripathi, A. K.; Scholl, P. F.; Shuman, J.; Bajad, S.; Shulaev, V.; Sullivan, D. J. The Role of Eutral Lipid Nanospheres in Plasmodium Falciparum Haem Crystallization. *Biochemical Journal* **2007**, *402* (1), 197–204. https://doi.org/10.1042/BJ20060986.

(13) Hoang, A. N.; Sandlin, R. D.; Omar, A.; Egan, T. J.; Wright, D. W. The Neutral Lipid Composition Present in the Digestive Vacuole of Plasmodium Falciparum Concentrates Heme and Mediates β-Hematin Formation with an Unusually Low Activation Energy. *Biochemistry* **2010**, *49* (47), 10107–10116. https://doi.org/10.1021/bi101397u.

(14) Carter, M. D.; Phelan, V. V; Sandlin, R. D.; Bachmann, B. O.; Wright, D. W. Lipophilic Mediated Assays for β-Hematin Inhibitors. *Comb Chem High Throughput Screen* **2010**, *13* (3), 285–292.

(15) Sandlin, R. D.; Carter, M. D.; Lee, P. J.; Auschwitz, J. M.; Leed, S. E.; Johnson, J. D.; Wright, D. W. Use of the NP-40 Detergent-Mediated Assay in Discovery of Inhibitors of β-Hematin Crystallization. *Antimicrob Agents Chemother* **2011**, *55* (7), 3363–3369. https://doi.org/10.1128/AAC.00121-11.

(16) Sandlin, R. D.; Fong, K. Y.; Stiebler, R.; Gulka, C. P.; Nesbitt, J. E.; Oliveira, M. P.; Oliveira, M. F.; Wright, D. W. Detergent-Mediated Formation of β-Hematin: Heme Crystallization Promoted by Detergents Implicates Nanostructure Formation for Use as a Biological Mimic. *Cryst Growth Des* **2016**, *16* (5), 2542–2551. https://doi.org/10.1021/acs.cgd.5b01580.

(17) Huy, N. T.; Uyen, D. T.; Maeda, A.; Trang, D. T. X.; Oida, T.; Harada, S.; Kamei, K. Simple Colorimetric Inhibition Assay of Heme Crystallization for High-Throughput Screening of Antimalarial Compounds. *Antimicrob Agents Chemother* **2007**, *51* (1), 350–353. https://doi.org/10.1128/AAC.00985-06.

(18) Huy, N. T.; Maeda, A.; Uyen, D. T.; Trang, D. T. X.; Sasai, M.; Shiono, T.; Oida, T.; Harada, S.; Kamei, K. Alcohols Induce Beta-Hematin Formation via the Dissociation of Aggregated Heme and Reduction in Interfacial Tension of the

Solution. *Acta Trop* **2007**, *101* (2), 130–138. https://doi.org/10.1016/j.actatropica.2007.01.001.

(19) Pasternack, R. F.; Munda, B.; Bickford, A.; Gibbs, E. J.; Scolaro, L. M. On the Kinetics of Formation of Hemozoin, the Malaria Pigment. *J Inorg Biochem* **2010**, *104* (10), 1119–1124. https://doi.org/10.1016/j.jinorgbio.2010.07.001.

(20) Vekilov, P. G.; Rimer, J. D.; Olafson, K. N.; Ketchum, M. A. Lipid or Aqueous Medium for Hematin Crystallization? *CrystEngComm* **2015**, *17* (41), 7790–7800. https://doi.org/10.1039/c5ce01178g.

(21) Adams, P. A.; Egan, T. J.; Ross, D. C.; Silver, J.; Marsh, P. J. *The Chemical Mechanism of β-Haematin Formation Studied by Mo$ Ssbauer Spectroscopy*; 1996; Vol. 318.

(22) Egan, T. J.; Chen, J. Y. J.; de Villiers, K. A.; Mabotha, T. E.; Naidoo, K. J.; Ncokazi, K. K.; Langford, S. J.; McNaughton, D.; Pandiancherri, S.; Wood, B. R. Haemozoin (β-Haematin) Biomineralization Occurs by Self-Assembly near the Lipid/Water Interface. *FEBS Lett* **2006**, *580* (21), 5105–5110. https://doi.org/10.1016/j.febslet.2006.08.043.

(23) Avrami M. Kinetics of Phase Change. I. *Journal of Chemical Physics* **1939**, *7* (12), 1103–1112.

(24) Egan, T. J.; Ncokazi, K. K. Quinoline Antimalarials Decrease the Rate of β-Hematin Formation. *J Inorg Biochem* **2005**, *99* (7), 1532–1539. https://doi.org/10.1016/j.jinorgbio.2005.04.013.

(25) Gildenhuys, J.; Roex, T. Le; Egan, T. J.; De Villiers, K. A. The Single Crystal X-Ray Structure of β-Hematin DMSO Solvate Grown in the Presence of Chloroquine, a β-Hematin Growth-Rate Inhibitor. *J Am Chem Soc* **2013**, *135* (3), 1037–1047. https://doi.org/10.1021/ja308741e.

(26) Fitzroy, S. M.; Gildenhuys, J.; Olivier, T.; Tshililo, N. O.; Kuter, D.; De Villiers, K. A. The Effects of Quinoline and Non-Quinoline Inhibitors on the Kinetics of Lipid-Mediated β-Hematin Crystallization. *Langmuir* **2017**, *33* (30), 7529–7537. https://doi.org/10.1021/acs.langmuir.7b01132.

(27) Egan, T. J.; Tshivhase, M. G. Kinetics of β-Haematin Formation from Suspensions of Haematin in Aqueous Benzoic Acid. *Dalton Transactions* **2006**, No. 42, 5024–5032. https://doi.org/10.1039/b610866k.

(28) Olafson, K. N.; Ketchum, M. A.; Rimer, J. D.; Vekilov, P. G. Mechanisms of Hematin Crystallization and Inhibition by the Antimalarial Drug Chloroquine. *Proc*

Natl Acad Sci U S A **2015**, *112* (16), 4946–4951. https://doi.org/10.1073/pnas.1501023112.

(29) Rifaie-Graham, O.; Hua, X.; Bruns, N.; Balog, S. The Kinetics of β-Hematin Crystallization Measured by Depolarized Light Scattering. *Small* **2018**, *1802295*, 1–7.

(30) Ali, M. E.; Oppeneer, P. M. Unraveling the Electronic Structure, Spin States, Optical and Vibrational Spectra of Malaria Pigment. *Chemistry - A European Journal* **2015**, *21* (23), 8544–8553. https://doi.org/10.1002/chem.201406208.

(31) Ncokazi, K. K.; Egan, T. J. A Colorimetric High-Throughput β-Hematin Inhibition Screening Assay for Use in the Search for Antimalarial Compounds. *Anal Biochem* **2005**, *338* (2), 306–319. https://doi.org/10.1016/j.ab.2004.11.022.

(32) Lagarec, K.; Rancourt, D. G. RECOIL 1.05. Mössbauer Spectral Analysis Software for Windows. University of Ottawa 1998.

(33) Lutterotti, L. Total Pattern Fitting for the Combined Size-Strain-Stress-Texture Determination in Thin Film Diffraction. *Nucl Instrum Methods Phys Res B* **2010**, *268* (3–4), 334–340. https://doi.org/10.1016/j.nimb.2009.09.053.

(34) Pagola S; Stephens W; Bohle S; Kosar A; Madsen S. The Structure of malaria Pigment β-Haematin. *Letters to Nature* **2000**, *404*, 307–310.

(35) Enkovaara, J.; Rostgaard, C.; Mortensen, J. J.; Chen, J.; Dułak, M.; Ferrighi, L.; Gavnholt, J.; Glinsvad, C.; Haikola, V.; Hansen, H. A.; Kristoffersen, H. H.; Kuisma, M.; Larsen, A. H.; Lehtovaara, L.; Ljungberg, M.; Lopez-Acevedo, O.; Moses, P. G.; Ojanen, J.; Olsen, T.; Petzold, V.; Romero, N. A.; Stausholm-Møller, J.; Strange, M.; Tritsaris, G. A.; Vanin, M.; Walter, M.; Hammer, B.; Häkkinen, H.; Madsen, G. K. H.; Nieminen, R. M.; Nørskov, J. K.; Puska, M.; Rantala, T. T.; Schiøtz, J.; Thygesen, K. S.; Jacobsen, K. W. Electronic Structure Calculations with GPAW: A Real-Space Implementation of the Projector Augmented-Wave Method. *Journal of Physics Condensed Matter*. 2010. https://doi.org/10.1088/0953-8984/22/25/253202.

(36) Perdew, J. P.; Burke, K.; Ernzerhof, M. Generalized Gradient Approximation Made Simple. *Physical Review Letter* **1996**, *77* (18), 3865–3868.

(37) Tkatchenko, A.; Scheffler, M. Accurate Molecular van Der Waals Interactions from Ground-State Electron Density and Free-Atom Reference Data. *Phys Rev Lett* **2009**, *102* (7). https://doi.org/10.1103/PhysRevLett.102.073005.

(38) Porezag, D.; Pederson, M. R. Infrared Intensities and Raman-Scattering Activities within Density-Functional Theory. *Phys Rev B* **1996**, *54* (11), 7830–7836.

(39) Buller, R.; Peterson, M. L.; Almarsson, Ö.; Leiserowitz, L. Quinoline Binding Site on Malaria Pigment Crystal: A Rational Pathway for Antimalaria Drug Design. *Cryst Growth Des* **2002**, *2* (6), 553–562. https://doi.org/10.1021/cg025550i.

(40) Solomonov, I.; Osipova, M.; Feldman, Y.; Baehtz, C.; Kjaer, K.; Robinson, I. K.; Webster, G. T.; McNaughton, D.; Wood, B. R.; Weissbuch, I.; Leiserowitz, L. Crystal Nucleation, Growth, and Morphology of the Synthetic Malaria Pigment β-Hematin and the Effect Thereon by Quinoline Additives: The Malaria Pigment as a Target of Various Antimalarial Drugs. *J Am Chem Soc* **2007**, *129* (9), 2615–2627. https://doi.org/10.1021/ja0674183.

(41) Dilanian, R. A.; Streltsov, V.; Coughlan, H. D.; Quiney, H. M.; Martin, A. V.; Klonis, N.; Dogovski, C.; Boutet, S.; Messerschmidt, M.; Williams, G. J.; Williams, S.; Phillips, N. W.; Nugent, K. A.; Tilley, L.; Abbey, B. Nanocrystallography Measurements of Early Stage Synthetic Malaria Pigment. *J Appl Crystallogr* **2017**, *50* (5), 1533–1540. https://doi.org/10.1107/S1600576717012663.

(42) Straasø, T.; Kapishnikov, S.; Kato, K.; Takata, M.; Als-Nielsen, J.; Leiserowitz, L. The Role of the Four Stereoisomers of the Heme Fe-O Cyclic Dimer in the Crystalline Phase Behavior of Synthetic Hemozoin: Relevance to Native Hemozoin Crystallization. *Cryst Growth Des* **2011**, *11* (8), 3342–3350. https://doi.org/10.1021/cg200410b.

(43) Straasø, T.; Marom, N.; Solomonov, I.; Barfod, L. K.; Burghammer, M.; Feidenhans'L, R.; Als-Nielsen, J.; Leiserowitz, L. The Malaria Pigment Hemozoin Comprises at Most Four Different Isomer Units in Two Crystalline Models: Chiral as Based on a Biochemical Hypothesis or Centrosymmetric Made of Enantiomorphous Sectors. *Cryst Growth Des* **2014**, *14* (4), 1543–1554. https://doi.org/10.1021/cg401151f.

(44) Marom, N.; Tkatchenko, A.; Kapishnikov, S.; Kronik, L.; Leiserowitz, L. Structure and Formation of Synthetic Hemozoin: Insights from First-Principles Calculations. *Cryst Growth Des* **2011**, *11* (8), 3332–3341. https://doi.org/10.1021/cg200409d.

(45) Reilly, J. T.; Walsh, J. M.; Greenfield, M. L.; Donohue, M. D. Analysis of FT-IR Spectroscopic Data: The Voigt Profile. *Spectrochimica Acta* **1992**, *48* (10), 1459–1479.

(46) Belafhal, A. The Shape of Spectral Lines: Widths and Equivalent Widths of the Voigt Profile. *Opt Commun* **2000**, *177*, 111–118.

(47) Hanssen, E.; Knoechel, C.; Klonis, N.; Abu-Bakar, N.; Deed, S.; LeGros, M.; Larabell, C.; Tilley, L. Cryo Transmission X-Ray Imaging of the Malaria Parasite, P. Falciparum. *J Struct Biol* **2011**, *173* (1), 161–168. https://doi.org/10.1016/j.jsb.2010.08.013.

(48) Bakar, N. A.; Klonis, N.; Hanssen, E.; Chan, C.; Tilley, L. Digestive-Vacuole Genesis and Endocytic Processes in the Early Intraerythrocytic Stages of Plasmodium Falciparum. *J Cell Sci* **2010**, *123* (3), 441–450. https://doi.org/10.1242/jcs.061499.

(49) de Villiers, K. A.; Kaschula, C. H.; Egan, T. J.; Marques, H. M. Speciation and Structure of Ferriprotoporphyrin IX in Aqueous Solution: Spectroscopic and Diffusion Measurements Demonstrate Dimerization, but Not μ-Oxo Dimer Formation. *JBIC Journal of Biological Inorganic Chemistry* **2007**, *12* (1), 101–117. https://doi.org/10.1007/s00775-006-0170-1.

(50) Klonis, N.; Dilanian, R.; Hanssen, E.; Darmanin, C.; Streltsov, V.; Deed, S.; Quiney, H.; Tilley, L. Hematin−Hematin Self-Association States Involved in the Formation and Reactivity of the Malaria Parasite Pigment, Hemozoin. *Biochemistry* **2010**, *49* (31), 6804–6811. https://doi.org/10.1021/bi100567j.

(51) Matz, J. M.; Drepper, B.; Blum, T. B.; Van Genderen, E.; Burrell, A.; Stach, T.; Collinson D , L. M.; Abrahams, J. P.; Matuschewski, K.; Blackman, M. J.; Beverley, S. M. A Lipocalin Mediates Unidirectional Heme Biomineralization in Malaria Parasites. *PNAS* **2020**, *117* (28), 16546–16556. https://doi.org/10.1073/pnas.2001153117/-/DCSupplemental.

(52) Crespo, M. P.; Tilley, L.; Klonis, N. Solution Behavior of Hematin under Acidic Conditions and Implications for Its Interactions with Chloroquine. *Journal of Biological Inorganic Chemistry* **2010**, *15* (7), 1009–1022. https://doi.org/10.1007/s00775-010-0661-y.

(53) Zill, D. G.; Cullen, M. R. Chapter 3, Section 3.2, Nonlinear Models. In *Differential Equations with Boundary-Value Problems*; Brooks/Cole, 1986.

(54) Delpe Acharige, A. M. D. S.; Brennan, M. P. C.; Lauder, K.; McMahon, F.; Odebunmi, A. O.; Durrant, M. C. Computational Insights into the Inhibition of β-Haematin Crystallization by Antimalarial Drugs. *Dalton Transactions* **2018**, *47* (43), 15364–15381. https://doi.org/10.1039/C8DT03369B.

(55) Largitte, L.; Pasquier, R. A Review of the Kinetics Adsorption Models and Their Application to the Adsorption of Lead by an Activated Carbon. *Chemical Engineering Research and Design* **2016**, *109*, 495–504. https://doi.org/https://doi.org/10.1016/j.cherd.2016.02.006.

(56) Syafiuddin, A.; Salmiati, S.; Jonbi, J.; Fulazzaky, M. A. Application of the Kinetic and Isotherm Models for Better Understanding of the Behaviors of Silver Nanoparticles Adsorption onto Different Adsorbents. *J Environ Manage* **2018**, *218*, 59–70. https://doi.org/https://doi.org/10.1016/j.jenvman.2018.03.066.

TABLES

Table 1. Kinetic equations explored in the present investigation.

	Model	Equation	Comments	Ref.
1	Zero order	$y = y_0 + k_0 t$	Independent upon the concentration of hemin.	[21]
2	Order 1	$y = y_0\left[1 - exp(-k_1 t)\right]$	Depends upon the hemin concentration.	[27]
3	Avrami	$y = y_0\left[1 - exp\left(-k_A t^n\right)\right]$	Consider both nucleation and growth of crystals.	[8]

4	Order 1 and Avrami	$y = y_0 - y_1 exp\left(-k_1 t\right) - y_2 exp\,(-k_A t$	Combines first order and Avrami models.	[19]
5	Modified Gompertz	$y = y_0 - \left(y_0 - y_1\right) exp\,[-exp\{a - b$ $a = \left(\frac{\mu}{y_0 - y_1}\right)\lambda + 1$ $b = \left(\frac{\mu}{y_0 - y_1}\right)$	Empirical model used for the description of biological phenomena such as the growth of tumors, and crystallization of fats and oils.	[27]
6	Modified Avrami	$y = y_0\left\{1 - exp\left[-\frac{z_0}{(c[Q]+1)^2}t^2\right]\right\}$	Incorporates the concentration of the antimalarial as a variable in one term of the Avrami equation.	[24]
7	Avrami - Langmuir	$y = \frac{100k_A}{k_A + k_2[D]^2 + k_2 K_{ads}[D]^3}$ $\left\{1 - exp\left[-\left(\frac{k_A + k_2[D]^2 + k_2 K_{ads}[D]^3}{1 + K_{ads}[D]}\right)t\right]\right\}$	Combines the crystallization characteristics of Avrami equation, and the interaction between the surface of the crystal and the antimalarial medicine as described by a Langmuir isotherm.	[25]
8	Avrami - Langmuir II	$y = \frac{100Yk_A}{k_A + k_2[D]^2 + k_2 K_{ads}[D]^3}$ $\left\{1 - exp\left[-\left(\frac{k_A + k_2[D]^2 + k_2 K_{ads}[D]^3}{1 + K_{ads}[D]}\right)t\right]\right\}$	Same as the previous one, but incorporates a parameter related to the maximal yield of β-hematin formed in the	[26]

			absence of the antimalarial.	
9	Second Order	$y = y_0 - \frac{1}{kt + c}$	Second order Kinetics on hemin concentration or on dimer concentration. The process of two hemin or dimers assembling in the solution.	[52]
10	Logistic	$y = \frac{Cy_0\, exp(y_0 kt)}{1 + C\, exp(y_0 kt)}$	A second order kinetic in which a dimer adheres to the surface of an already formed crystal.	[53]
11	Second Order + Logistic	$y = \frac{c_1 y_0\, exp(y_0 k_1 t)}{1 + c_1\, exp(y_0 k_1 t)} + y_1 - \frac{1}{k_2 t + c_2}$	Combination of the process of nucleation and crystal growth.	This work

Table 2. The statistical analysis for the goodness of fit of the kinetic curves was performed by using the error functions shown here.[55,56] N is the number of data points. $y_{exp,i}$ is the measured % conversion of hemin to β-hematin for the i-th data. y_i is the calculated % conversion of hemin to β-hematin for the i-th data. $\underline{y_{exp}}$ is the average of the measured % conversion of hemin to β-hematin data.

Error function	Equation
Determination coefficient	$R^2 = \frac{\sum_{i=1}^{N}\left(y_{exp,i} - \underline{y_{exp}}\right)^2 - \sum_{i=1}^{N}\left(y_{exp,i} - y_i\right)^2}{\sum_{i=1}^{N}\left(y_{exp,i} - \underline{y_{exp}}\right)^2}$
Root of the mean squared error	$RMSE = \sqrt{\frac{1}{N}\sum_{i=1}^{N}\left(y_{exp,i} - y_i\right)^2}$
Mean absolute percentage error	$MAPE = \left(\frac{1}{N}\sum_{i=1}^{N}\frac{\left\lvert y_{exp,i} - y_i\right\rvert}{\left\lvert y_{exp,i}\right\rvert}\right) x\, 100\%$

Table 3. Errors obtained from fitting the experimental kinetic curves by using the models reported in Table 1 and using the formulas reported in Table 2.

Model	β-hematin			β-hematin + Cq 0,565 mM			β-hematin + Cq 1,667 mM		
	R^2	RMSE	MAPE	R^2	RMSE	MAPE	R^2	RMSE	MAPE
Order 1	0,96	6,85	21,64	0,98	3,42	17,69	0,95	5,02	20,16
Avrami	0,99	3,02	14,71	0,99	0,97	14,62	0,97	4,09	18,78
Order 1-Avrami	0,99	0,64	1,12	0,99	0,50	0,34	0,99	2,24	2,77
Modified Avrami	0,99	3,22	1,81	0,84	13,42	26,85	0,85	9,38	26,61
Avrami-Langmuir I	0,96	6,85	21,64	0,98	3,42	17,69	0,95	5,02	20,16
Avrami-Langmuir II	0,96	6,85	21,64	0,98	3,42	17,69	0,95	5,02	20,16
Modified Gompertz	0,99	2,60	6,29	0,99	0,53	0,35	0,96	4,76	12,53
Second Order	0,94	8,02	24,40	0,98	4,64	8,96	0,97	4,15	7,35
Logistic	0,99	1,86	6,07	0,99	1,32	8,98	0,91	7,00	19,58
Second order + Logistic	0,99	0,57	0,46	0,99	0,52	0,35	0,99	2,23	2,70

Table 4.1. Kinetics parameters of the linear combination of Order 1 and Avrami models, in the equation 4 reported in Table 1. The parameter y_0 is related with the maximum yield, or percentage of formation of β-hematin from hemin; k_A and k_1 are the kinetic constants for the Avrami and Order 1 parts of the equation, respectively.

Parameter	β-hematin	β-hematin + Cq 1,667 mM
y_0 (%)	100 ± 1	78 ± 6
y_1 (%)	45 ± 6	48 ± 9
y_2 (%)	51 ± 4	27 ± 11
k_A (h^{-1})	0,41 ± 0,05	0,02 ± 0,07
k_1 (h^{-1})	0,98 ± 0,11	25,02 ± 0,01
n	4,00 ± 0,45	3,99 ± 3,67

Table 4.2. Some kinetics parameters of the linear combination of Second order and Logistic models, in the equation 11 reported in Table 1. The parameters C_1 and C_2 are the integration constants; k_1 and k_2 are the kinetic constants for the Logistic and Second order parts of the equation, respectively.

Parameter	β-hematin	β-hematin + Cq 1,667 mM
y_0 (%)	58 ± 5	25 ± 74
y_1 (%)	49 ± 8	55 ± 92

k_1 (h^{-1})	0,08 ± 0,01	0,1 ± 0,6
k_2 (h^{-1})	0,02 ± 0,01	0,24 ± 5,80
C_1	0,005 ± 0,002	0,001 ± 0,002
C_2	0,020 ± 0,004	0,01 ± 0,02

Table 5. Crystallographic unit cell parameters derived from the Rietveld analysis of the PXRD patterns using the MAUD program.[33] For comparison purposes, the cell parameters reported by Pagola et al.[34] are also included.

Sample	Cell parameters reported by Pagola et al.[34]	β-hematin	β-hematin + Cq 0,565 mM	β-hematin + Cq 1,667 mM
a (Å)	12,2	12,239	12,228	12,12
b (Å)	14,7	14,780	14,820	14,797
c (Å)	8,0	8,091	8,088	8,074

α *(°)*	90,2	90,676	90,289	90,717
β *(°)*	96,8	96,560	96,704	96,655
γ *(°)*	97,9	98,230	97,928	98,190
Vol(Å)	1410,822	1438,454	1441,431	1423,178

Table 6. Ratios of the intensities of (001) and (100) crystallographic planes relative to (020), (031) and (131) crystallographic planes for the different samples. The I_{001}/I_{hkl} and I_{100}/I_{hkl} ratios are denoted as $I_{001/hkl}$ and $I_{100/hkl}$, respectively. The intensity of a given Bragg peak was taken as the area of that peak.

Intensity **ratios**	$I_{001/020}$	$I_{001/031}$	$I_{001/131}$	$I_{100/020}$	$I_{100/031}$	$I_{100/131}$
β-hematin	0,55	0,23	0,18	2,28	0,97	0,76
β-hematin + Cq 0,565 mM	0,81	0,19	0,16	4,10	0,96	0,82
β-hematin + Cq 1,667 mM	0,49	0,18	0,16	2,44	0,91	0,81

Table 7. Ratios of the mean coherence lengths L_{001} and L_{100} along the 001 and 100 directions with respect to the mean coherence lengths L_{020}, L_{031} and L_{131} along the 020, 031 and 131 directions for the different samples investigated. The L_{001}/L_{hkl} and L_{100}/L_{hkl} ratios are denoted $L_{001/hkl}$, and $L_{100/hkl}$, respectively. The L_{hkl} values were calculated by applying the Scherrer formula $L_{hkl} = 0,9 \times 2\pi/FWHM_{hkl}$, where $FWHM_{hkl}$ is the full-width at half maximum for each Bragg peak.[40]

Size ratios	$L_{001/020}$	$L_{001/031}$	$L_{001/131}$	$L_{100/020}$	$L_{100/031}$	$L_{100/131}$
$_{\beta}$-hematin	0,83	0,83	0,67	1,46	1,45	1,16
β-hematin + Cq 0,565 mM	0,67	1,34	1,00	0,79	1,60	1,20
β-hematin + Cq 1,667 mM	0,83	1,17	0,84	1,25	1,75	1,25

Table 8.1 Positions and relative intensities of some selected infrared bands located in the spectral regions of 1000 – 2000 cm^{-1}, and of 2000 – 4000 cm^{-1}. The intensities for the bands in the 1000 – 2000 cm^{-1} region are relative to the intensity of the 1206 cm^{-1} band, whereas in the 2000 – 4000 cm^{-1} region are with respect to the 2850 cm^{-1} band.

β-hematin		β-hematin + Cq 0,565 mM		β-hematin + Cq 1,667 mM		Assignation
Position (cm^{-1})	**Relative Area**	**Position (cm^{-1})**	**Relative Area**	**Position (cm^{-1})**	**Relative Area**	
1206	1	1207	1	1209	1	Esters/Stretching/ C-O (Fe)
1661	0,36	1661	0,71	1662	0,47	Carboxyl/ Stretching/Link between porphyrin rings
1711	0,42	1711	0,75	1712	0,80	Carboxyl/ Stretching/Link between dimers
2850	1	2859	1	2859	1	Amines/Stretching/ N–CH2
2917	0,95	2919	4,98	2910	0,83	Amines/Stretching/ N–CH2
3299	0,64	3100	0,85	3100	1,14	O-H / Stretching

Table 8.2 Positions of the IR molecular vibrations of the β-hematin predicted by the theoretical calculations.

Molecular Vibration	Description	Theoretical Wave Number (cm^{-1})

Esters /Stretching	C-O (Fe)	1165 - 1171
Porphyrin	C-N, C-C	1489 - 1493
Carboxyl/ Stretching	C=O Link between porphyrin rings	1643 - 1646
Carboxyl/ Stretching	C=O Link between dimers	1768
CC, C - H Stretching	Vinyls and Methyls	2937 - 3179
O-H in Carboxyl	H-O between dimers	3632 - 3636

Table 9. Average crystal sizes, height and width, and height to width ratio calculated from the SEM micrographs, for the β-hematin synthesized in absence and in presence of chloroquine at 0,565 mM and 1,667 mM concentrations.

Dimension (nm)	**β-hematin**	**β-hematin + Cq 0,565 mM**	**β-hematin + Cq 1,667 mM**
Height	767 ± 64	717 ± 71	347,05 ± 46
Width	141 ± 21	114 ± 20	345 ± 5
Height/Width ratio	5,44 ± 0,93	6,29 ± 1,27	1,01 ± 0,13

FIGURE CAPTIONS

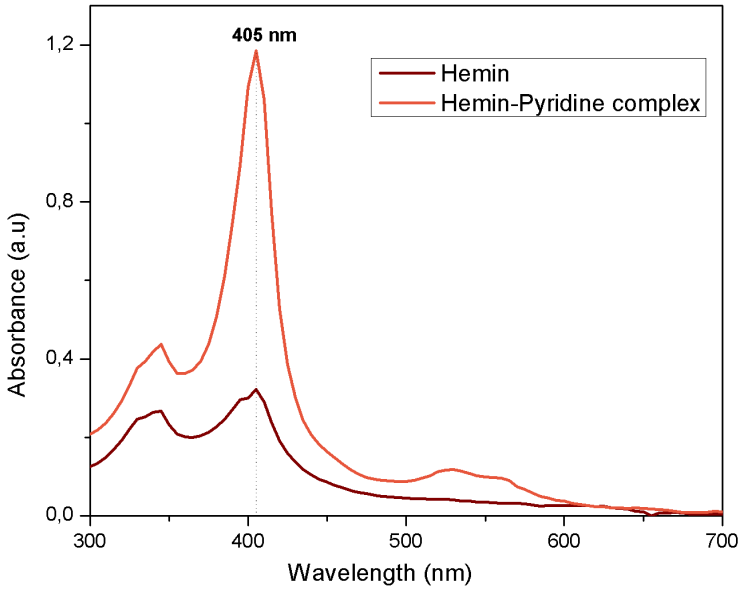

Figure 1. UV-Vis spectrum of hemin and hemin-pyridine complex.

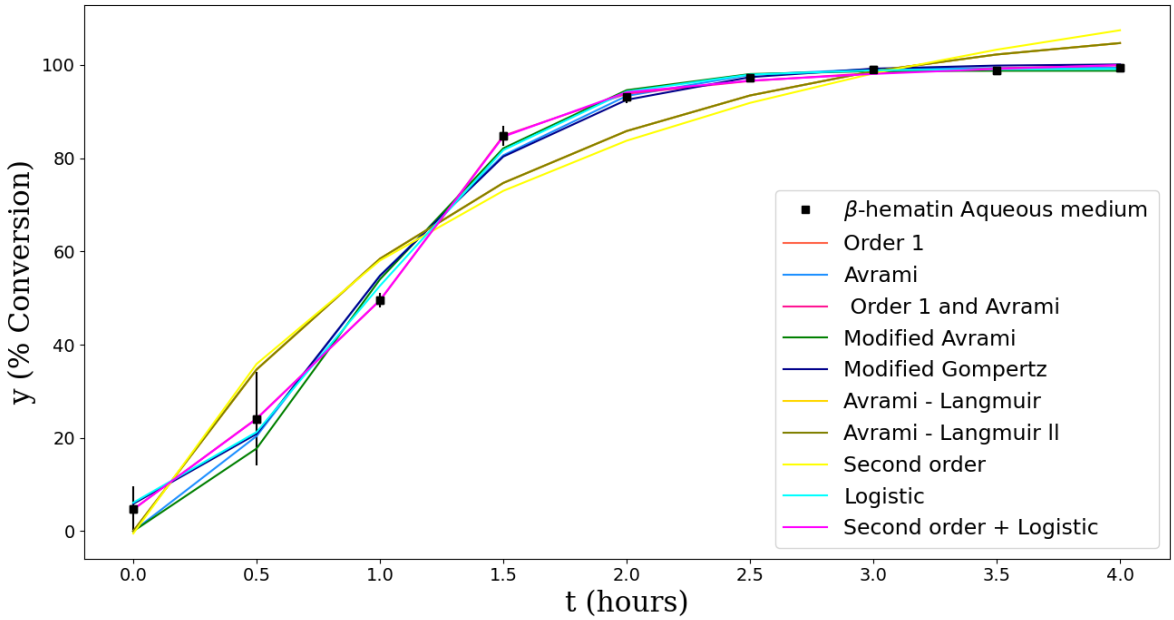

Figure 2. Comparison of the different models used to fit the kinetic data of β-hematin crystallization when it is synthesized in absence of chloroquine. The experimental data (black squares symbols) represent the average of three independent experiments (error bars are shown).

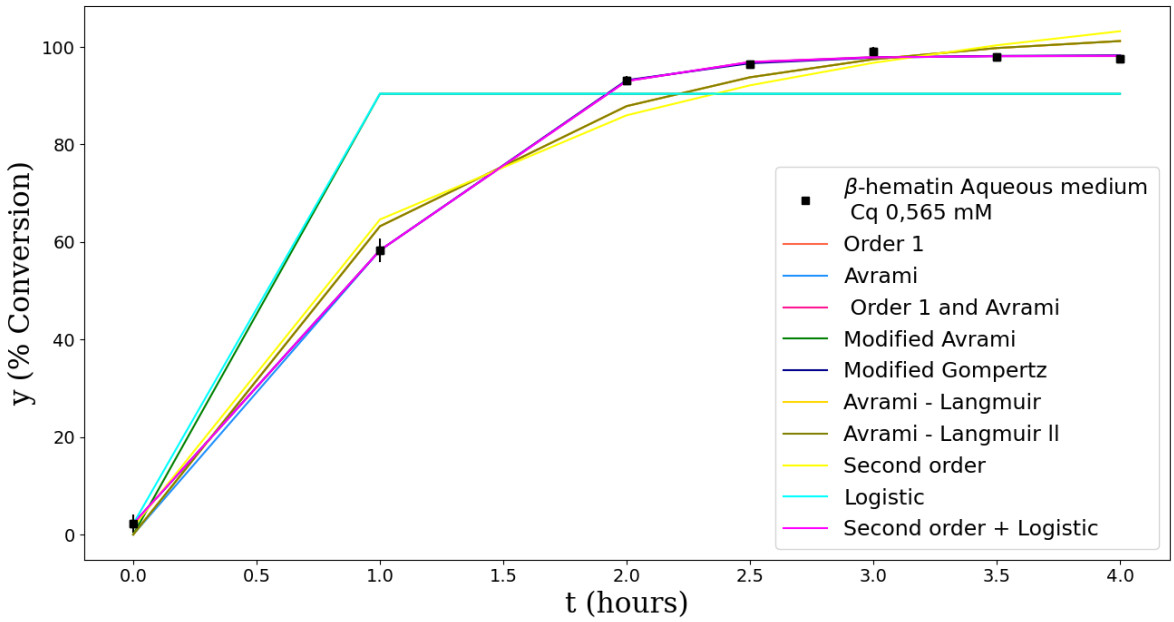

Figure 3. Comparison of the different models used to fit the kinetic data of β-hematin crystallization when it is synthesized in presence of 0,565 mM chloroquine. The experimental data (black squares symbols) represent the average of three independent experiments (error bars are shown).

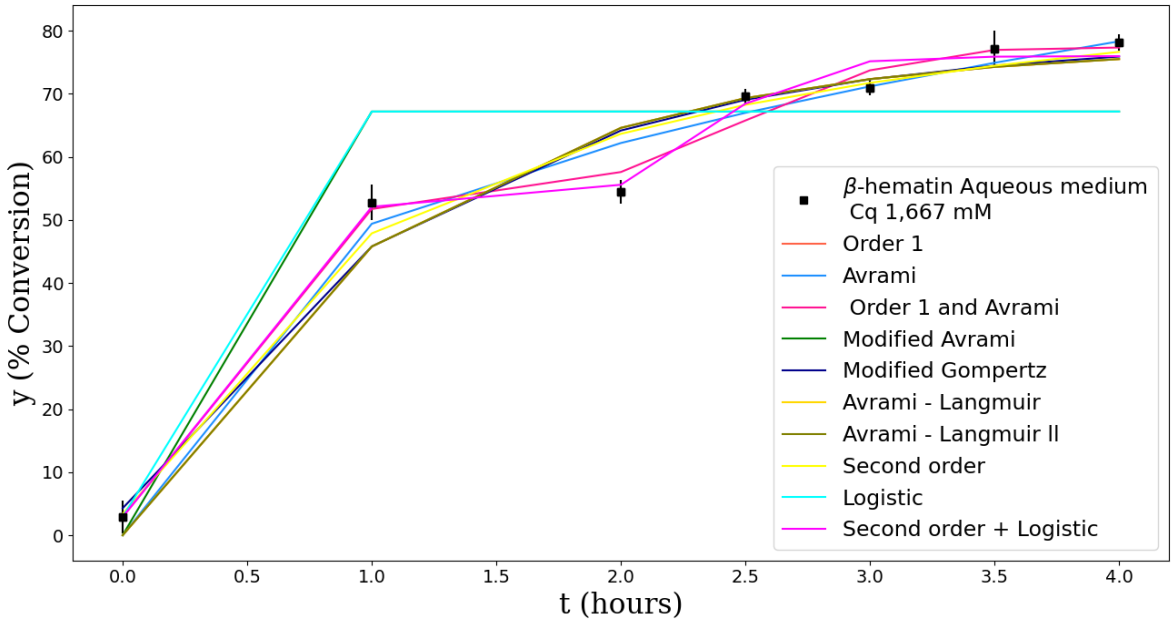

Figure 4. Comparison of the different models used to fit the kinetic data of β-hematin crystallization when it is synthesized in presence of 1,667 mM chloroquine. The experimental data (black squares symbols) represent the average of three independent experiments (error bars are shown).

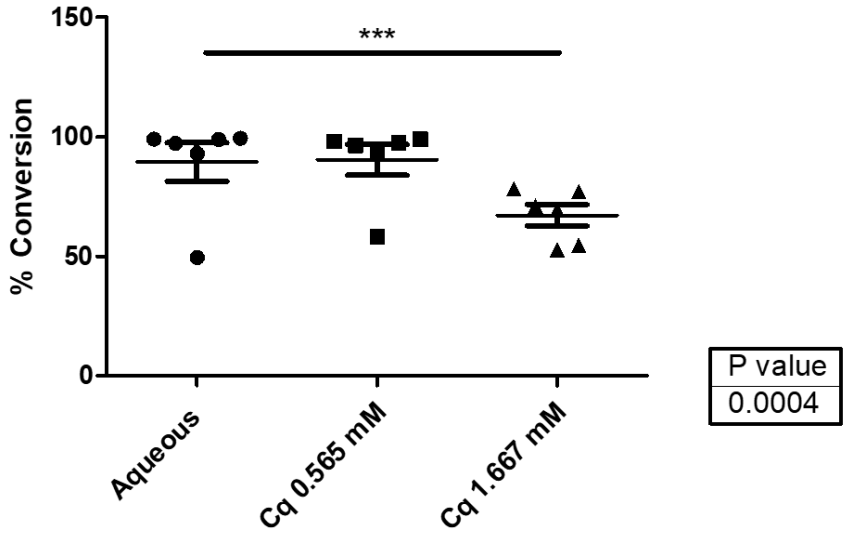

Figure 5. Comparative conversion of hemin to β-hematin with different concentrations of chloroquine.

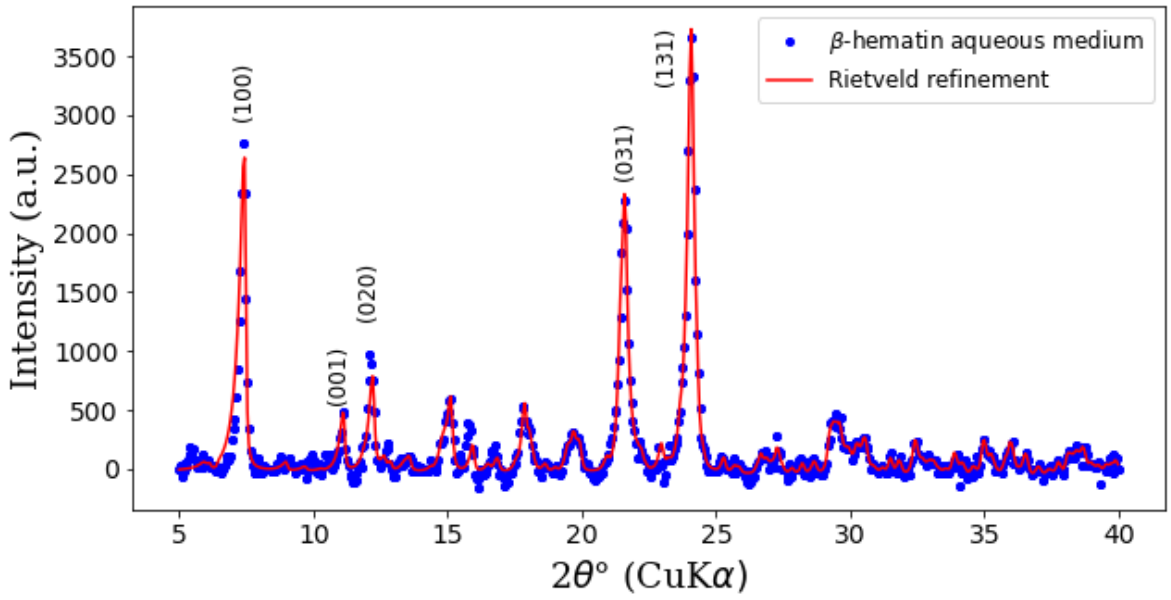

Figure 6. PXRD pattern of β-hematin synthesized in aqueous medium. The blue filled circles and the red lines represent the experimental data and the calculated pattern using the MAUD program, respectively. The Miller indices of some Bragg peaks are indicated.

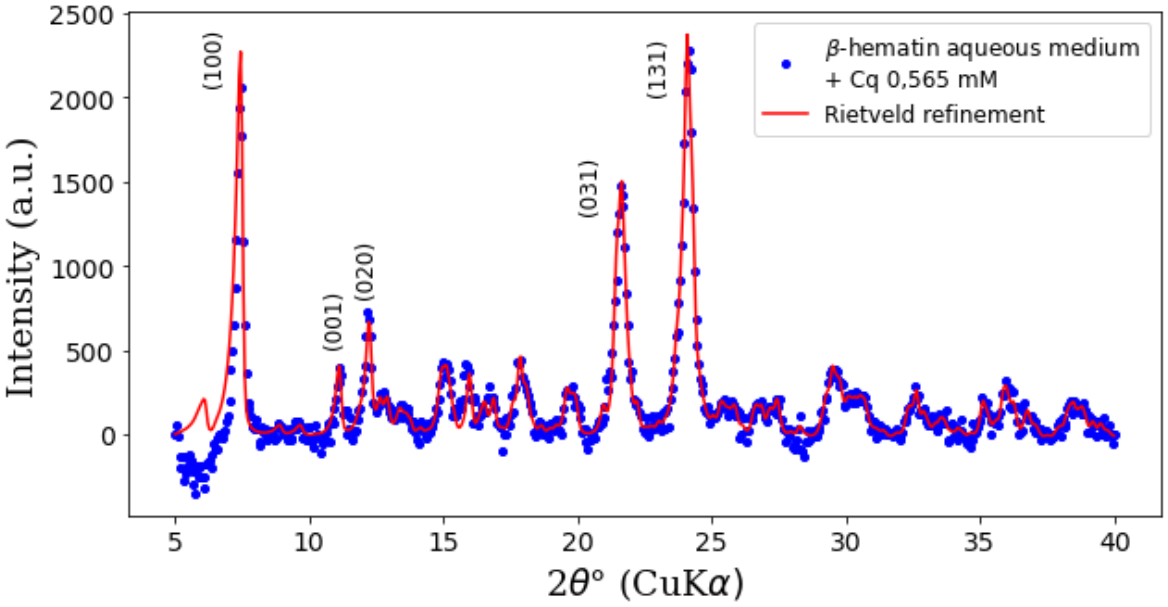

Figure 7. PXRD pattern of β-hematin synthesized in aqueous medium in presence of 0,565 mM chloroquine. The blue filled circles and the red lines represent the experimental data

and the calculated pattern using the MAUD program, respectively. The Miller indices of some Bragg peaks are indicated.

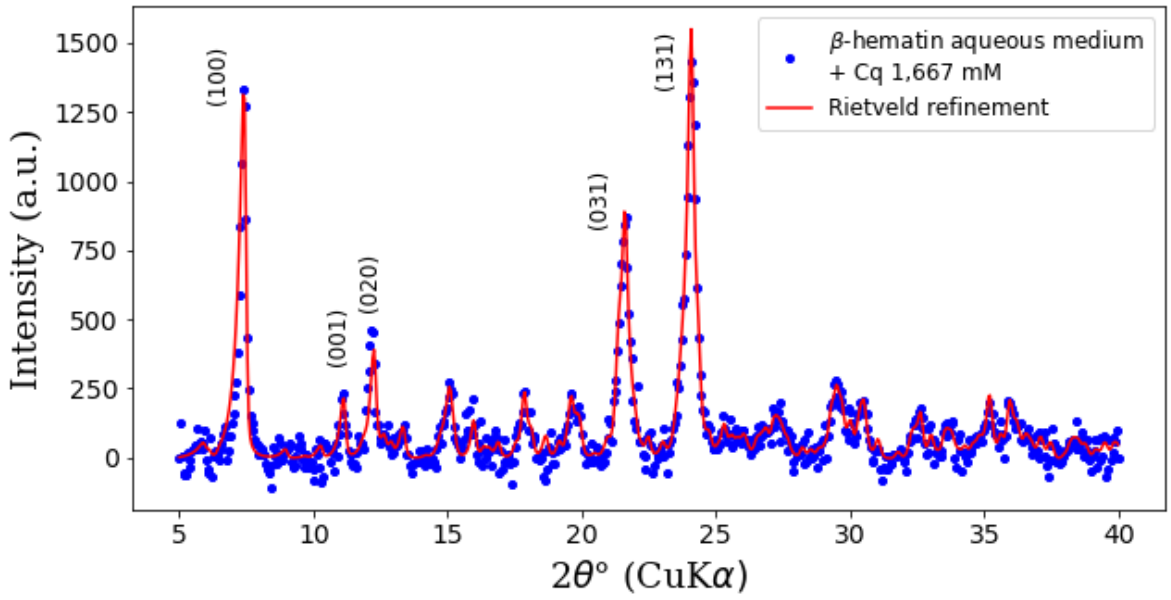

Figure 8. PXRD pattern of β-hematin synthesized in aqueous medium in presence of 1,667 mM chloroquine. The blue filled circles and the red lines represent the experimental data and the calculated pattern using the MAUD program, respectively. The Miller indices of some Bragg peaks are indicated.

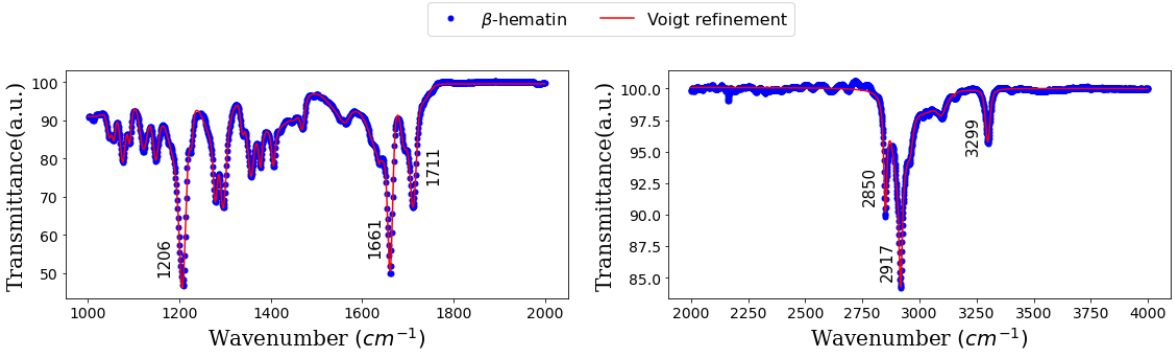

Figure 9. FTIR spectrum of β-hematin obtained in aqueous medium in absence of chloroquine. With the purpose to simplify the fitting, the spectrum was divided into three spectral regions. In this figure we show the 1000-2000 cm^{-1} (left) and 2000-4000 cm^{-1} (right) regions. The blue filled circles represent the experimental data, while the continuous red lines are the fitted IR spectra using the Voigt function as implemented in the RECOIL program[32].

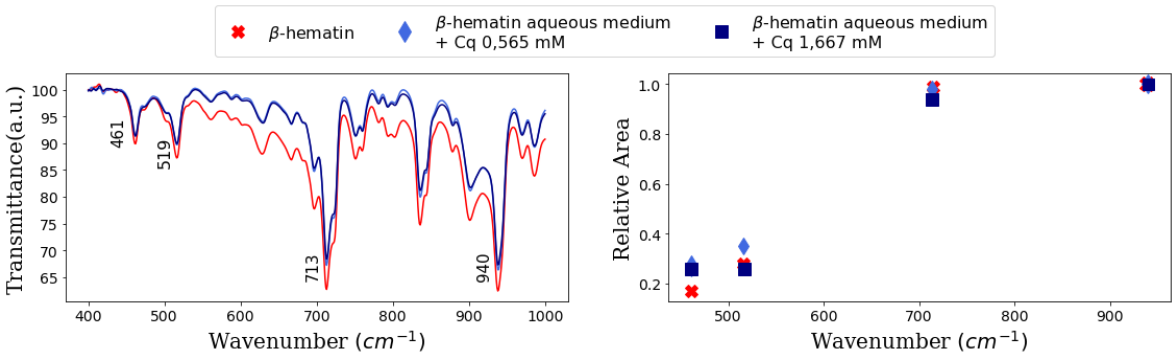

Figure 10. (left side) FTIR spectra in the range from 400 to 1000 cm^{-1} for β-hematin (red), β-hematin prepared in presence of 0,565 mM chloroquine (light blue) and β-hematin prepared in the presence of 1,667 mM chloroquine (dark blue). (right side) Areas of bands located at 461 cm^{-1}, 517 cm^{-1} and 713 cm^{-1} with respect to the area of the band at 940 cm^{-1} for the three samples investigated.

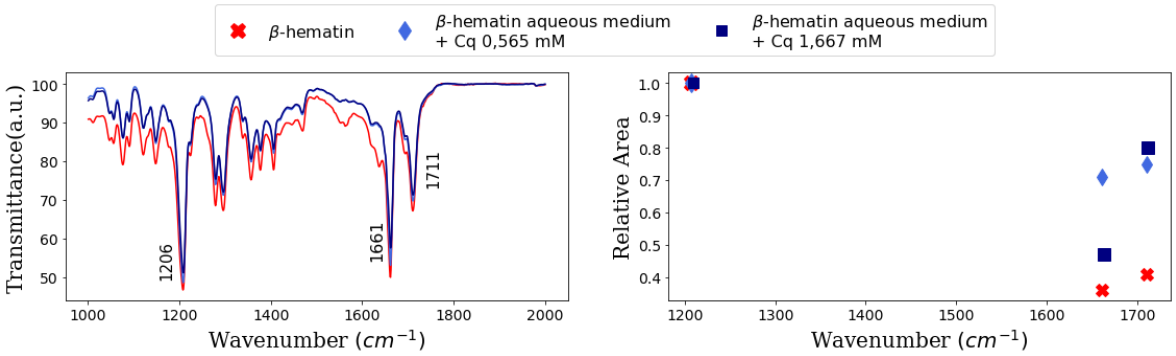

Figure 11. (left side) FTIR spectra in the range from 1000 to 2000 cm^{-1} for β-hematin (red), β-hematin prepared in presence of 0,565 mM chloroquine (light blue) and β-hematin prepared in the presence of 1,667 mM chloroquine (dark blue). (right side) Areas of bands located at 1661 cm^{-1} and 1711 cm^{-1} with respect to the area of the band at 1206 cm^{-1} for the three samples investigated.

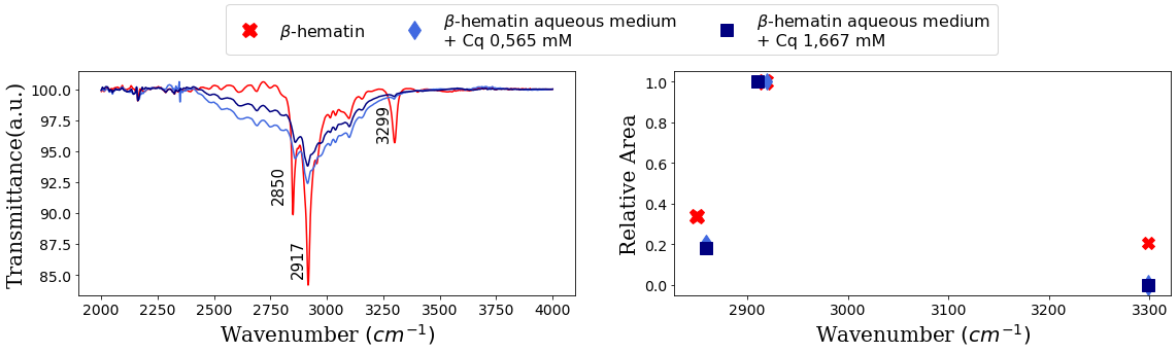

Figure 12. (left side) FTIR spectra in the range from 2000 to 4000 cm^{-1} for β-hematin (red), β-hematin prepared in presence of 0,565 mM chloroquine (light blue) and β-hematin prepared in the presence of 1,667 mM chloroquine (dark blue). (right side) Areas of bands located at 2917 cm^{-1} and 3299 cm^{-1} with respect to the area of the band at 2850 cm^{-1} for the three samples investigated.

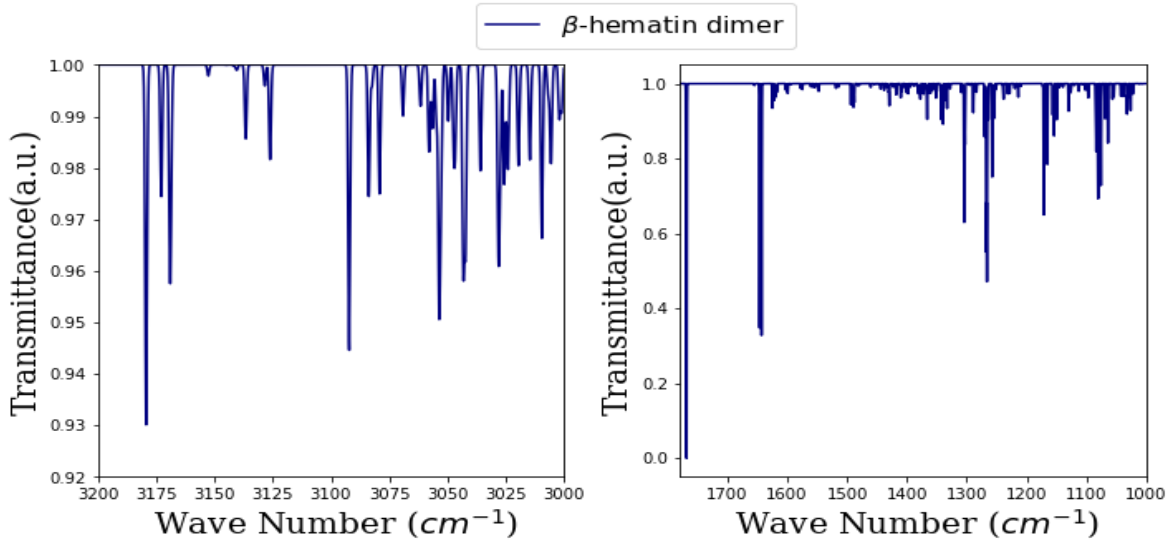

Figure 13. Simulated FTIR spectra of a hemin dimer as a model of β-hematin.

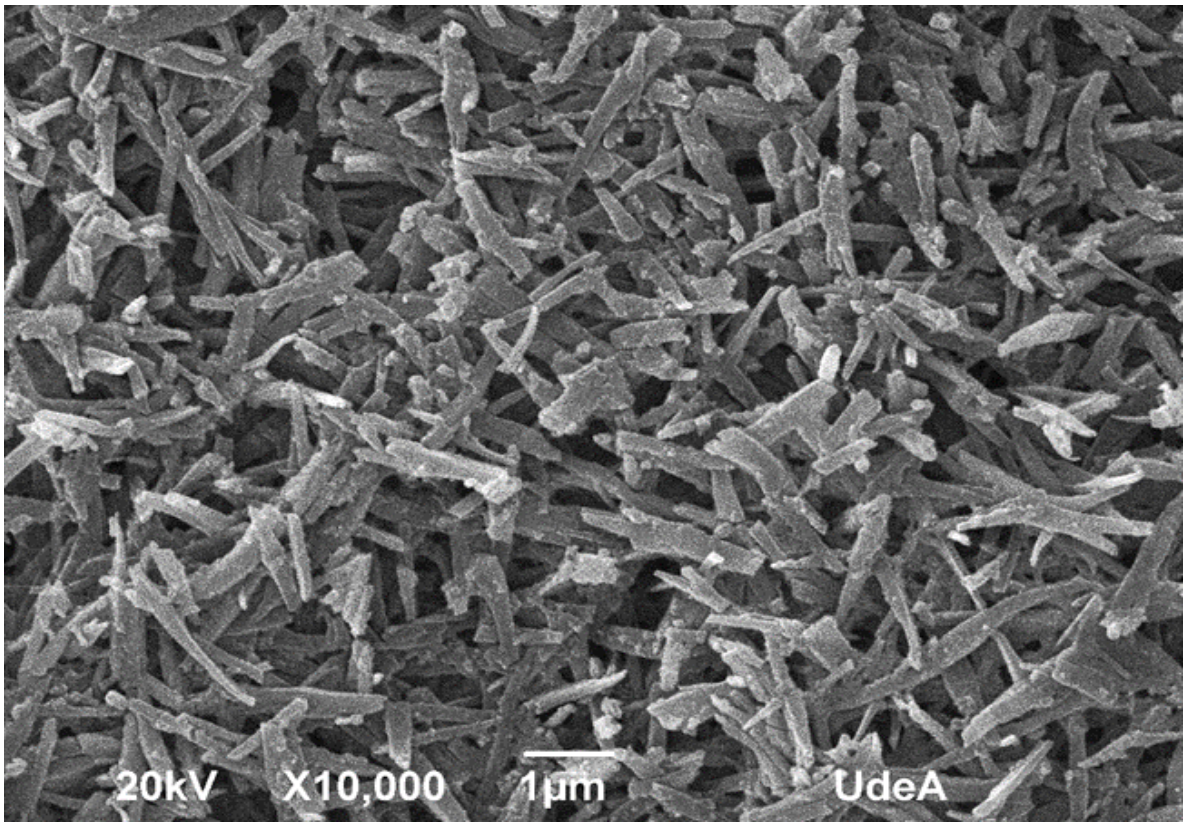

Figure 14: SEM micrograph of the β-hematin sample synthesized in the absence of chloroquine.

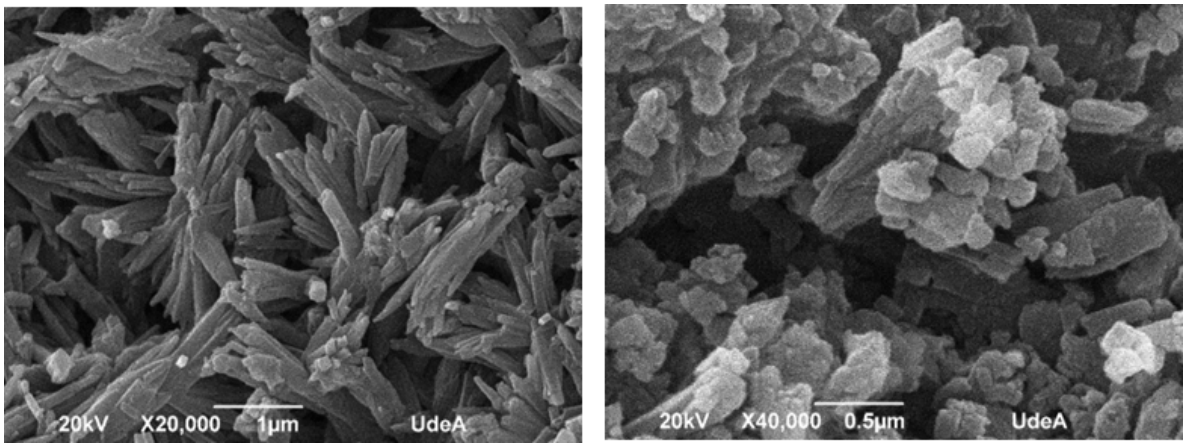

Figure 15: SEM micrograph of the β-hematin sample synthesized in the presence of 0,565 mM chloroquine.

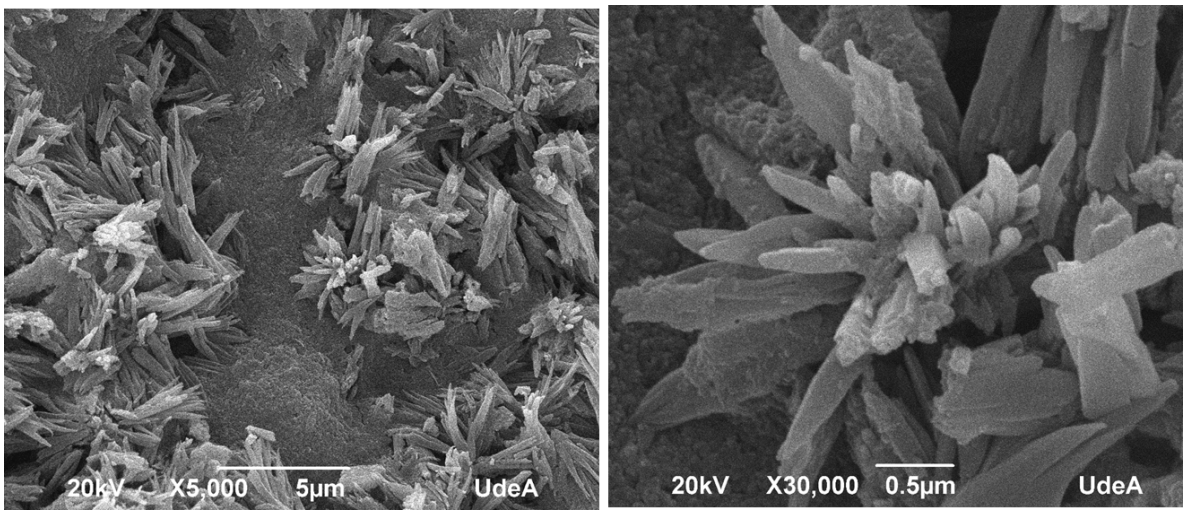

Figure 16: SEM micrograph of the β-hematin sample synthesized in the presence of 1,667 mM chloroquine.

Table of Contents Graphic

Synopsis

Our manuscript investigates the mechanisms of β-hematin crystallization and chloroquine inhibition by using kinetic studies and physico-chemical quantitative characterization and simulation.

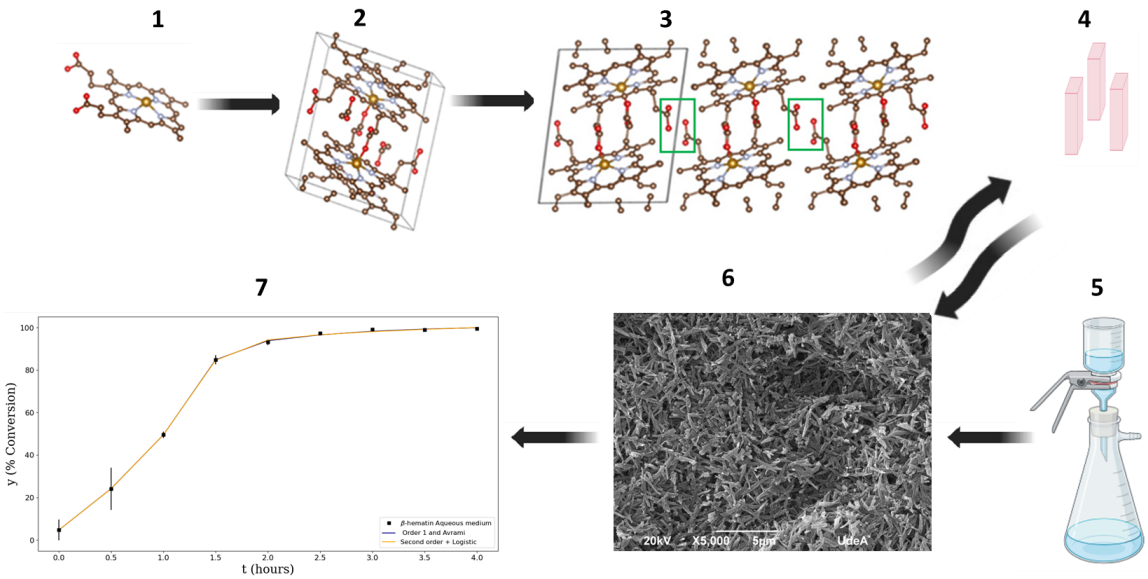

1. Hemin precursor. 2. β-hematin dimer. 3. Assembling of performed dimers. 4. Theorical morphology of the crystal. 5. Obtaining synthetic hemozoin. 6. Synthetic Hemozoin (β-hematin) SEM. 7. Best kinetic models.